Atmos. Meas. Tech. Discuss., 8, 8385–8437, 2015
www.atmos-meas-tech-discuss.net/8/8385/2015/
doi:10.5194/amtd-8-8385-2015

Atmospheric Measurement Techniques Discussions
Open Access

Impact of aerosols on the OMI tropospheric NO_2 retrievals over industrialized regions: how accurate is the aerosol correction of cloud-free scenes via a simple cloud model?

J. Chimot[1], T. Vlemmix[1], J. P. Veefkind[1,2], J. F. de Haan[2], and P. F. Levelt[1,2]

[1]Department of Geoscience and Remote Sensing (GRS), Civil Engineering and Geosciences, TU Delft, the Netherlands
[2]Royal Netherlands Meteorology Institute, De Bilt, the Netherlands

Received: 3 June 2015 – Accepted: 21 July 2015 – Published: 10 August 2015

Correspondence to: J. Chimot (j.j.chimot@tudelft.nl)

Published by Copernicus Publications on behalf of the European Geosciences Union.

Abstract

The Ozone Monitoring Instrument (OMI) instrument has provided daily global measurements of tropospheric NO_2 for more than a decade. Numerous studies have drawn attention to the complexities related to measurements of tropospheric NO_2 in the presence of aerosols. Fine particles affect the OMI spectral measurements and the length of the average light path followed by the photons. However, they are not explicitly taken into account in the current OMI tropospheric NO_2 retrieval chain. Instead, the operational OMI O_2-O_2 cloud retrieval algorithm is applied both to cloudy scenes and to cloud free scenes with aerosols present. This paper describes in detail the complex interplay between the spectral effects of aerosols, the OMI O_2-O_2 cloud retrieval algorithm and the impact on the accuracy of the tropospheric NO_2 retrievals through the computed Air Mass Factor (AMF) over cloud-free scenes. Collocated OMI NO_2 and MODIS Aqua aerosol products are analysed over East China, in industrialized area. In addition, aerosol effects on the tropospheric NO_2 AMF and the retrieval of OMI cloud parameters are simulated. Both the observation-based and the simulation-based approach demonstrate that the retrieved cloud fraction linearly increases with increasing Aerosol Optical Thickness (AOT), but the magnitude of this increase depends on the aerosol properties and surface albedo. This increase is induced by the additional scattering effects of aerosols which enhance the scene brightness. The decreasing effective cloud pressure with increasing AOT represents primarily the absorbing effects of aerosols. The study cases show that the actual aerosol correction based on the implemented OMI cloud model results in biases between −20 and −40 % for the DOMINO tropospheric NO_2 product in cases of high aerosol pollution (AOT $\geq$ 0.6) and elevated particles. On the contrary, when aerosols are relatively close to the surface or mixed with NO_2, aerosol correction based on the cloud model results in overestimation of the DOMINO tropospheric NO_2 product, between 10 and 20 %. These numbers are in line with comparison studies between ground-based and OMI tropospheric NO_2 measurements under conditions with high aerosol pollution and elevated particles. This

AMTD
8, 8385–8437, 2015

highlights the need to implement an improved aerosol correction in the computation of tropospheric NO_2 AMFs.

1 Introduction

Nitrogen oxides ($NO_x = NO + NO_2$) play a key role in atmospheric chemistry, regulating the level of ozone and maintaining the oxidizing capacity in the troposphere. The most important reasons to improve our knowledge of the global distributions of NO_x are (1) Exposure to nitrogen dioxide leads to adverse health impacts; (2) the chemical budget of tropospheric ozone, toxic also for humans and the vegetation, is largely determined by the concentration of NO_x (Jacob et al., 2006); (3) nitrogen oxides are the precursors of (ammonium) nitrate, an important component of particulate matter, and contribute to acidification and eutrophication of soils and surface waters; and, (4) nitrogen oxides affect the global climate indirectly by affecting OH, and therefore modifying the residence time of the greenhouse gases O_3 and CH_4 (Shindell et al., 2009). Over industrialized regions with comparable photochemical regimes, NO_x and aerosol concentrations are often very well correlated showing similar anthropogenic sources between aerosols and short-lived trace gases.

In 2004, the Dutch-Finnish Ozone Monitoring Instrument (OMI) (Levelt et al., 2006) was launched on the NASA EOS-Aura satellite. OMI is a nadir-viewing imaging spectrometer that provides with daily global coverage of key air quality components. The retrieval technique of the OMI tropospheric NO_2 Vertical Column Density (VCD) (Boersma et al., 2004) is common to all the other similar satellite missions (Burrows et al., 1999; Bovensmann et al., 1999). The backscattered solar radiation is captured in daylight in the visible spectral domain by the instrument at the Top Of the Atmosphere (TOA) and then processed through the Differential Optical Absorption Spectroscopy (DOAS) retrieval approach. The DOAS method is based on radiative transfer modelling of tropospheric NO_2 Air Mass factor (AMF). The associated assumptions play a crucial role on the accuracy of the tropospheric NO_2 VCD.

AMTD
8, 8385–8437, 2015

The DOMINO (Derivation of OMI tropospheric NO_2) (Boersma et al., 2011) product contain worldwide concentrations of NO_2 in the troposphere (0–12 km altitude) derived from OMI. This product is used by a large number of air quality studies like in (Curier et al., 2014; Reuter et al., 2014). The computation of tropospheric NO_2 AMF is acknowledged as the dominant source of errors in the retrieved tropospheric NO_2 column over polluted areas (Boersma et al., 2007) with important consequences to emission constraints and other applications. The overall uncertainty for individual retrievals of DOMINO tropospheric NO_2 vertical column densities is estimated to be 1.0×10^{15} molecules cm^{-2} (±25 %) (Boersma et al., 2011; Lin et al., 2014; Lamsal et al., 2014). Several studies that investigated the accuracy of the DOMINO products over rural and urban areas in Russia, Asia and Indonesia, by using different long-term network observations based on Multi-Axis Differential Optical Absorption Spectroscopy (MAX-DOAS). (Shaiganfar et al., 2011; Ma et al., 2013; Kanaya et al., 2014) found a negative bias between 26 and 50 % in urban and very polluted areas and when the Aerosol Optical Thickness (AOT) is high. These underestimations have been recently confirmed as well by (Wang et al., 2015b) over Wuxi city, area with high pollution adjoined to Shangai. These low biases could be partially attributed to the inhomogeneity of NO_2 at the spatial scale of OMI observation, and incomplete accounting of NO_2 near the surface. However, the possible additional effects caused by aerosols cannot be ignored. Over industrial regions with comparable photochemical regimes, NO_2 and aerosol concentrations are very well correlated showing similar anthropogenic sources between aerosols and short-lived trace gases (Veefkind et al., 2011). A proper characterization of aerosols' impact on the retrieval is then needed to accurately quantify trace gas amounts from satellite observations.

The current version of the DOMINO algorithm does not explicitly account for the aerosol effects on the tropospheric NO_2 AMF. Similarly, these effects are not explicitly considered in the other UV-Vis satellite measurements (Valks et al., 2011). Aerosols affect the top-of-atmosphere (TOA) radiances in the visible and O_2-O_2 spectral bands (Boersma et al., 2011; Leitão et al., 2010). The OMI cloud algorithm (Acarreta et al.,

AMTD
8, 8385–8437, 2015

2004) derives the cloud fraction and cloud pressure from the O_2-O_2 absorption in the spectral window between 460–490 nm. This cloud retrieval algorithm is applied both to cloudy and cloud-free scenes with aerosols. In other words, aerosols are treated as clouds. Studies (Boersma et al., 2004, 2011) mention that the correction for the aerosol impact cannot be simply separated from the effects of clouds and, if a cloud retrieval scheme is applied, it will account for a large part of the aerosol effect by retrieving modified cloud fraction and pressure. (Wang et al., 2015a) show that OMI cloud parameters are indeed perturbed in presence of aerosols, by comparing with classified sky conditions using MAX-DOAS observations. Therefore, the cloud retrievals apply an implicit correction of aerosols presence in the computation of the tropospheric NO_2. In spite of many studies evaluating the magnitude of the explicit aerosol correction on the computation of tropospheric NO_2 AMFs, little attention has been paid to the interplay between aerosol effects and OMI cloud retrieval algorithms. Moreover, the dependence of the retrieved cloud parameters and the associated implicit aerosol correction to the geophysical conditions and the aerosol properties are not clear. The needs to investigate further and understanding the interplay between all these variables have been highlighted in different studies (Leitão et al., 2010; Lin et al., 2014). It has recently been emphasized in (Castellanos et al., 2015) for the analyses of the implicit aerosol corrections in case of biomass burning aerosols.

This paper aims to analyse how aerosols currently affect the operational OMI cloud products and the derived tropospheric NO_2 AMFs. For that purpose, this study uses a model vs. observation approach focused on large industrialized areas in China. This work focuses on cloud-free scenes but dominated by aerosol pollution. The paper starts with a description of the expected aerosol net effects on the tropospheric NO_2 AMFs, based on simulations. The importance of aerosols and NO_2 vertical profiles is highlighted. In the next section, the OMI DOMINO v2 products are confronted to collocated MODIS aerosol products over large industrial area in China. This provides insights in the behaviour of OMI cloud fraction and pressure, and tropospheric NO_2 AMFs in the presence of aerosols. The following section summarises the simulated DOAS O_2-O_2

AMTD
8, 8385–8437, 2015

cloud retrieval results implemented and evaluated on aerosol cases, as achieved by the operational OMI algorithm,. The interplay between aerosol effects and the DOAS O_2-O_2 cloud retrieval can be characterized. In the last section, we deduce how an implicit aerosol correction is applied in the OMI retrieval chain through the Lambertian cloud model and evaluate its accuracy by comparing it to the explicit aerosol corrections simulated in Sect. 2.

2 Impact of aerosols on the tropospheric NO_2 AMF

This section starts with a description of how the tropospheric NO_2 AMF is computed. Then, we compare AMFs for scenes with and without aerosols.

2.1 Computation of the tropospheric NO_2 AMF

A two-step approach is used to determine the NO_2 Vertical Column Density (VCD). First, the DOAS method (Platt and Stutz, 2008), based on the basic principle of absorption spectroscopy and the Beer-Lambert law, is applied to the measured spectra within 405–465 nm in order to derive a NO_2 slant column density (SCD). This column gives the number of NO_2 molecules per cm^2, integrated along the average light path. Then, the NO_2 SCD is converted into NO_2 vertical column density (VCD). This can be done by application of the air mass factor (AMF) calculated with a radiative transfer model. The AMF A is defined as the ratio of the atmospheric SCD and VCD (Boersma et al., 2011):

$$A(\Psi) = N^{s}(\Psi)/N^{v}, \quad (1)$$

where N^s is the NO_2 SCD and N^v is the NO_2 VCD. The computation of $A(\Psi)$ requires accurate knowledge on the geophysical conditions, as they impact the length of light path followed by the backscattered sunlight. The list of variables describing these conditions is summarised by Ψ and is detailed in Table 1.

AMTD
8, 8385–8437, 2015

The concept of altitude-resolved AMF for an atmospheric layer (Wagner et al., 2007; Rozanov et al., 2010), also named block air mass factor or BAMF in other studies, allows to generalise this definition by computing this variable at discrete atmospheric layers such as:

$$a(p^*) = \left.\frac{\Delta N^s(\Psi)}{\Delta N^v}\right|_{\Delta n(p=p^*)}, \quad (2)$$

which describes the altitude dependence of A. a is the altitude-resolved AMF at atmospheric pressure p. $\Delta n(p = p^*)$ refers to a change in the trace gas profile n at pressure level p^*. ΔN^v and ΔN^s denote the resulting changes in VCD and SCD respectively. Currently, only cloud particles, and no aerosols, are considered when computing $a(p)$ in the DOMINO product. Figure 2 depicts an example of vertical distribution of $a(p)$ for a cloud-free observation at 439 nm. Without aerosols, $a(p)$ values generally decrease close to the surface. A is then computed by weighting $a(p)$ with the atmospheric vertical distribution of the trace gas profile:

$$A = \frac{\int_{p_0}^{p_{top}} a(p) \cdot n(p)\,\mathrm{d}p}{\int_{p_0}^{p_{top}} n(p)\,\mathrm{d}p}, \quad (3)$$

where $n(p)$ is the vertical distribution of trace gas density, p_{top} the top of the atmosphere and p_0 is the surface pressure. In this paper, we define A^{tr} as tropospheric NO_2 AMF, which can be calculated from Eq. (3) by taking a vertical profile $n(p)$ that is set to zero above the troposphere.Therefore, A^{tr} gives an indication of the sensitivity of the satellite measurement to the amount of NO_2 in the lowest atmospheric layers. Assuming identical shape of vertical NO_2 profile, a larger A^{tr} value expresses a higher sensitivity of the measurement while a reduced A^{tr} value indicates a decreased sensitivity. Indeed,

AMTD
8, 8385–8437, 2015

in those cases, a change in A^{tr} is directly associated with a change of $a(p)$ at the atmospheric levels where the trace gas is present. $a(p)$ is in theory spectrally dependent, but the spectral dependence in case of tropospheric NO_2 is very small. The reference wavelength considered in this paper is 439 nm (Boersma et al., 2011)

2.2 Qualitative description of aerosol optical effects

Similarly to cloud particles, scattering and absorbing effects induced by the presence of aerosol particles affect the total radiance observed by the satellite sensor and the light path distribution of detected photons. The presence of aerosols leads in general to higher radiance levels captured by the satellite sensor. This increase has a spectral variability depending on the aerosol properties. Its magnitude is however smaller in cases of a very bright surface and absorbing aerosols. The change of light path distribution has consequences on the sensitivity of the remote sensing measurement to the tropospheric NO_2 amount. This sensitivity can be either increased or decreased. Qualitatively, one can distinguish two effects that aerosols/clouds can have on the NO_2 absorption signal at the TOA (Leitão et al., 2010):

- Shielding effect: decreased sensitivity within and below the aerosol/cloud layers. The fraction of all detected photons that reaches the lowest part of the atmosphere (below the aerosol/cloud layer) is reduced compared to a cloud or aerosol free scene because of absorption and/or scattering of photons in the direction of the satellite.
- Enhancement (albedo) effect: increased sensitivity within and above the aerosol/cloud layers. The fraction of all detected photons that sample the higher part of the atmosphere (above the aerosol/cloud layer) is increased, compared to a cloud or aerosol free scene, because more photons are scattered in the direction of the satellite.

AMTD
8, 8385–8437, 2015

Both effects are illustrated in Fig. 2, where shielding and enhancement can be seen relative to the line for $\tau = 0$. The overall impact of aerosols on a measurement depends thus on the relative importance of the above mentioned effects, which depends mainly on aerosol optical properties, amounts, surface reflectance and the vertical distribution of the particles, and the NO_2 gas. The geometry parameters like θ_0 (solar zenith angle or SZA) and θ (viewing zenith angle or VZA), and scattering angle (i.e. aerosol phase function) have an impact also as they modify the length of the light path.

2.3 Quantitative description of the impact of aerosols properties, their vertical distribution, and NO_2 profile

2.3.1 Methodology

To study the effects of aerosols on A^{tr}, this study uses the DISAMAR (Determining Instrument Specifications and Analyzing Methods for Atmospheric Retrieval) software developed at KNMI (de Haan, 2011). This software package includes a radiative transfer model and can apply different retrieval methods, such as direct fitting (within an optimal estimation framework) and DOAS. The radiative transfer model is based on the DAK (Doubling Adding KNMI) model (de Haan et al., 1987; Stammes et al., 2001) and thus computes the reflectance and transmittance in the atmosphere using the adding/doubling method. This method calculates the internal radiation field in the atmosphere at levels to be specified by the user and takes into account Rayleigh scattering, trace gas absorption, and aerosol and cloud scattering. Scattering by aerosols is simulated with a Henyey–Greenstein scattering phase function $\Phi(\cos\Theta)$ (Hovenier and Hage, 1989):

$$\Phi(\cos\Theta) = \frac{1 - g^2}{(1 + g^2 - 2g\cos\Theta)^{3/2}}, \quad (4)$$

where Θ is the scattering angle, and $g = \langle\cos\Theta\rangle$ is the asymmetry parameter. In a standard case, an asymmetry parameter of $g = 0.7$ is used. Thus, in DISAMAR,

AMTD
8, 8385–8437, 2015

the Angstrom exponent α gives the spectral dependence of the AOT τ. In DISAMAR, $a(p)$ is determined analytically, based on the weighting functions of the reflectances (i.e. derivatives of the reflectances to absorption cross-section and trace gas density). Indeed, $a(p)$ for an atmospheric layer can be identified as the Jacobian of the forward model $\partial F/\partial n$. This term is independent of the tracer distribution for optically thin absorbers. This methodology is conceptually equivalent to the approach discussed in Sect. 2.1.

The simulations in this section are done for aerosol particles with α of 1.5 for fine particles and 0.5 for coarse particles, asymmetry parameter 0.7 and single scattering albedo (SSA) $\omega_0 = 0.95$ and 0.9, assuming different altitudes, surface albedos 0.05 and 0.07 (surface reflectance is assumed Lambertian), solar zenith angle (SZA) $\theta_0 = 25^\circ$ and viewing zenith angle (VZA) $\theta = 25^\circ$. The NO_2 profiles are taken from a model run where atmospheric chemistry and transport model TM5 has been integrated into the global climate model EC-Earth version 2.4 (van Noije et al., 2014). We defined the tropospheric AMF aerosol factor $f(\tau)$ as the ratio of the air mass factor with ($A(\tau)$) and without aerosols present ($A(\tau = 0)$).

$$f(\tau) = \frac{A^{\mathrm{tr}}(\tau)}{A^{\mathrm{tr}}(\tau = 0)}. \quad (5)$$

f can be interpreted as the factor by which the tropospheric NO_2 AMF of a clear scene should be adjusted to represent aerosol effects. In practice, such a factor cannot be accurately determined as not all required information, associated with instantaneous individual measurement, is available. Identical to the DOMINO product, A^{tr} is computed at 439 nm.

Figure 3 is an example of these computations following Eq. (5) based on all the individual NO_2 profiles generated by the TM5 model for the month of July 2006 at 12:00 (close to the OMI local observation time) over the region of East China (lat. 30–40°, long. 110–130°) (see Fig. 1). The error bars in the Figs. 3–5 represent the variability in f due to the variability of the TM5 NO_2 profiles over this region in the

AMTD
8, 8385–8437, 2015

month of July. The curves in these figures connect the average values of f per AOT bin.

2.3.2 Results

Figure 3 demonstrates that f lies in the range between 0.7 and 1.3. The total effect of aerosols (shielding or enhancement) depends strongly on the location of the particles in the atmospheric layers, and results from the computed $a(p)$ depicted in Fig. 2. Scattering of aerosols enhances the tropospheric NO_2 A up to 30 % for $\tau = 1.0$ when they are located within or below the NO_2 bulk (between the surface and 900 hPa). When a given amount is lifted to higher altitudes, aerosols thus apply a shielding effect (i.e. reduced sensitivity to the tropospheric NO_2 amount) up to 30 %. The variability of the NO_2 vertical distribution impacts the magnitude of these effects, around 10 % for $\tau = 1$.

In addition to the vertical distribution of the aerosol particles, the shape of the vertical NO_2 profile also significantly affects on the magnitude of f. In winter (e.g. January in Fig. 1), such profile shows higher absolute values of concentrations near the surface and more variability. Moreover, the profile shape (after normalisation to integrated total column) depicts a small difference with a higher dynamic between the surface and the atmosphere layer at 900 hPa. Figure 4a shows amplified enhancement effects (up to 40 % for aerosols between the surface and 950 hPa) and amplified shielding effects (up to 45 % for aerosols at very high altitude, between 600 and 700 hPa). The transition between a net shielding or enhancement effect is also closer to the surface compared to summer (close to 950 hPa) as the aerosols are well mixed with the tropospheric NO_2 bulk only below 950 hPa. The variability of the NO_2 profile, mostly in the tropospheric layers, have a larger impact in January, where the error bars indicate a variability of around 20 % for $\tau = 1.0$. The altitudes of tropospheric NO_2 and aerosols, and so the relative altitude between both, are thus the key drivers of f.

Other parameters also contribute to the magnitude of this correction:

AMTD
8, 8385–8437, 2015

- An increase of surface albedo (cf. Fig. 3b), from 0.05 to 0.07, reduces the enhancement effect with 10 % and enhances the shielding effect with less than 5 % for $\tau = 1.0$.
- The size of particles specified through α has little impact on the aerosol correction (cf. Fig. 5a). Decreasing α from 1.5 (fine particles) to 0.5 (coarse particles) reduces the shielding and enhancement effects between 2 and 5 % for $\tau = 1.0$.
- A change of ω_0 from 0.95 to 0.9 (cf. Fig. 5b) leads to a reduction of the enhancement effect by 10 % (when aerosols are located below or well mixed with the tropospheric NO_2 bulk). The shielding effect is increased by 5 %.
- The increase of θ_0 from 25 to 50° (typically Winter average over China), increases the shielding effects by 10 % for $\tau = 1.0$ (assuming NO_2 profiles in January). Moreover, the enhancement effect increases between 5 and 10 % for τ between 0.3 and 0.7.
- The variability of the NO_2 profiles increases the variability of f when aerosols are located between 900 and 1000 hPa.

3 Interplay between aerosols and the OMI O_2–O_2 cloud retrievals

This section explains the perturbations induced by the aerosol particles on the retrieval of cloud fraction and cloud pressure based on the OMI O_2–O_2 spectral band. This section is structured as follows: firstly the OMI DOMINO product is analysed in confrontation with the MODIS Aqua aerosol product. Then, the OMI DOAS cloud O_2–O_2 retrieval chain is analysed with simulated aerosol cases.

3.1 Confrontation of OMI DOMINO-v2 with MODIS Aqua aerosol product

MODIS (Moderate Resolution Imaging Spectroradiometer) on-board EOS-Aqua observes the Earth's atmosphere approximately 15 min prior to OMI onboard EOS-Aura.

AMTD
8, 8385–8437, 2015

The aerosol effects on the current OMI tropospheric NO_2 retrievals are investigated by confronting collocated OMI DOMINO with MODIS Aqua Level 2 (L2) aerosol products over large industrialized areas in China. Statistics are computed over three years (2005–2007) for two seasons: summer (June, July and August) and winter (December, January and February). MODIS L2 aerosol products have a spatial resolution of 10 km × 10 km, close then to the OMI spatial resolution (13 km × 24 km at nadir). The OMI and MODIS data are paired on a pixel-by-pixel basis if the distance between pixel centers is less than 5 km and if both observations are acquired within 15 min. Observations with a cloud fraction higher than 0.1 are filtered out. This threshold is applied to both OMI and MODIS, although both parameters are not identical. Applying such a threshold on the observations increases the probability to identify cloud-free scenes. Moreover, the availability of the MODIS aerosol product is a good confirmation of the identification of cloud-free scenes as MODIS Aqua AOTs τ are retrieved exclusively for cloud-free situations (Remer et al., 2008). However, it is well recognised, according to the analyses in the next section, that cloud-free observations with large presence of aerosols are filtered out as well. Tests have been performed with higher cloud fraction thresholds (0.2 and 0.3) showing then no significant changes in the results described below.

The tropospheric NO_2 AMF that is extracted from the OMI DOMINO database, show a decreasing trend with increasing τ in Summer. This decrease is in average 5 % for MODIS $\tau = 1$, with a variability of 20 %. A small local positive trend (around 5 %) is however noticed for $\tau = 0$–0.2. On the contrary, in Winter, there is on average no modification of the tropospheric NO_2 A with increasing τ. By making use of the Angstrom coefficient α available in MODIS AQUA data (cf. Fig. 6c), it is found that tropospheric NO_2 A is larger for coarse particles than for fine particles (differences of 10 %).

Figures 7–9 depict the impact of aerosols on the OMI O_2–O_2 cloud fraction and pressure. Under aerosol presence and no cloud contamination in the OMI measurement, the OMI cloud fraction shows a clear linear relation with respect to τ. On average, values increase from 0.01 to 0.07 with a variability of 30 % for $\tau = 1$. The magnitude of

AMTD
8, 8385–8437, 2015

this increase depends on the surface albedo (Kleipool et al., 2008) and MODIS Aqua aerosol properties:

- The increase of cloud fraction with increasing AOT is higher over dark surfaces and lower over bright surfaces (average differences of 0.03 for $\tau = 1$, between OMI surface albedos of 0.04 and 0.08 (cf. Fig. 8);
- loud fraction values are higher in the presence of small particles (average differences of 0.03 between MODIS Aqua α of [1.5:1.8] and [0.4:0.8]) (cf. Fig. 9).

The cloud pressure values show a non-linear decrease from 800 to 600 hPa (in average) for $\tau = 1$, with a variability of around 100 hPa during Summer. However, no decrease is observed during Winter. The cloud pressure stays close to the surface (between 900 and 1000 hPa). The retrieved cloud pressures seem to have some sensitivity to the surface and aerosol properties. In particular, it decreases more over dark surface (difference of 100 hPa between surface albedo 0.04 and 0.07 for $\tau = 1$) and in the presence of fine particles.

Based on the OMI cloud and AMFs parameters observed in the DOMINO product for scenes dominated by aerosols, it can be seen that the cloud parameters respond to the presence of aerosols. One may conclude that there is an implicit correction for the presence of aerosols. On average, this correction applies a shielding effect in summer: i.e. the measurements are assumed to have less sensitivity to tropospheric NO_2 in the presence of aerosols.

3.2 Qualitative description of the OMI cloud algorithm

3.2.1 Inverse cloud model

In the context of trace gas measurements from space, the purpose of a cloud model is to describe the clouds in a way that reproduces the reflectance spectrum, and thus the distribution of photon paths, for cloudy-scenes. For this purpose, the parameters

AMTD
8, 8385–8437, 2015

designing such a model are cloud fraction, cloud optical thickness, cloud top altitude, and cloud vertical extent. However, instruments like OMI have limited spatial resolution (13 km × 24 km at nadir view) and do not resolve individual clouds. Therefore, cloud fraction and cloud optical thickness cannot be separated. Furthermore, OMI cannot give information on cloud microphysic properties such as cloud phase, cloud particle shape and size, and cloud vertical structure.

Because clouds are a correction step in trace gas retrievals, both the cloud retrieval algorithm and the cloud correction algorithm have to use the same cloud model. As a consequence, a simple model is used in the OMI tropospheric NO_2 retrievals, describing a cloud as a Lambertian reflector with a fixed albedo through which no light is transmitted. The associated effective cloud fraction is thus not a geometric cloud fraction but the radiometrically equivalent cloud fraction which, in combination with the assumed cloud albedo, yields a TOA reflectance that agrees with the observed reflectance. While scattering clouds have two main optical properties in the UV-Visible (namely reflection and transmission – their absorption being negligible), a Lambertian reflector has only reflection properties, determined by the cloud albedo, and no transmission properties. The OMI cloud retrieval algorithm assumes a cloud albedo of 0.8 (Stammes et al., 2008). This value has been found suitable to correct NO_2 and O_3 retrievals for partially cloudy scenes. The missing transmission of optically thin and medium thick clouds in the Lambertian cloud model is compensated for by the cloud-free part of the pixel.

Based on the properties of an opaque Lambertian cloud model, the effective cloud fraction is mainly constrained by the brightness of the cloud and how much a brighter cloud would outshine the observation scene. The effective cloud pressure is mainly constrained by the perturbation of the clouds on the O_2–O_2 collision complex absorption. A high cloud shields the O_2–O_2 complexes located below the cloud. As a consequence, the O_2–O_2 absorption signal is attenuated reflectance (Acarreta et al., 2004; Stammes et al., 2008; Sneep et al., 2008).

AMTD
8, 8385–8437, 2015

3.2.2 Description of the O_2-O_2 DOAS retrieval algorithm

The OMI cloud retrieval chain (Acarreta et al., 2004) exploits the 460–490 nm absorption band of O_2-O_2, a collision pair of oxygen. The retrieval algorithm is based on the DOAS method and consists of two steps. In the first step, the absorption cross-section spectrum of O_2-O_2 is fitted together with a first order polynomial to the negative logarithm of the measured reflectance spectrum. The window of the spectral fit is (460–490 nm) following:

$$-\ln(R) = \gamma_1 + \gamma_2 \cdot \lambda + N^{s}_{O_2-O_2}(\lambda) \cdot \sigma_{O_2-O_2} + N^{s}_{O_3}(\lambda) \cdot \sigma_{O_3}, \quad (6)$$

where $\gamma_1 + \gamma_2 \cdot \lambda$ defines the first order polynomial, $\sigma_{O_2-O_2}$ is the O_2-O_2 absorption cross-section spectrum (at 253 K), σ_{O_3} is the O_3 absorption cross section spectrum, $N^{s}_{O_3}$ is the O_3 slant column density density and $N^{s}_{O_2-O_2}$ is the O_2-O_2 slant column density density. The O_3 cross section spectrum is included because it overlaps with the O_2-O_2 spectrum. The fitted parameters are γ_1, γ_2, $N^{s}_{O_2-O_2}$, and $N^{s}_{O_3}$. In the absence of absorbers, one may define the continuum reflectance R_c at wavelength λ_0:

$$R_c = \exp(-\gamma_1 - \gamma_2 \cdot \lambda_0). \quad (7)$$

The reference wavelength is fixed at the middle of the DOAS fit window at $\lambda_0 = 475$ nm.

In the second step, a look-up-table is used to convert the retrieved $N^{s}_{O_2-O_2}$ and R_c into the cloud pressure C_p and cloud fraction C_f. This inversion step requires prior information about surface albedo, surface altitude and geometry angles (θ_0, θ and the relative azimuth angle $\phi - \phi_0$).

3.3 OMI cloud retrievals applied to aerosol scenes

To test the sensitivity to aerosols, the OMI DOAS O_2-O_2 algorithm was applied to simulated spectra for scenes dominated by aerosols. The implementation was performed in such a way that it is almost identical to the operational DOMINO chain at

AMTD
8, 8385–8437, 2015

KNMI. The effective cloud fraction and cloud pressure parameters are derived following Eqs. (6) and (7) and through linear interpolation in the look-up-table, assuming thus an opaque Lambertian cloud model described previously. Reflectance spectra are simulated by including only aerosol particles with the DISAMAR software. No clouds are included in the simulated reflectances. The sensitivity of the retrievals are investigated as a function of surface albedo, aerosol properties (α, ω_0, vertical distribution), θ_0 and θ. Simulated reflectances are noise-free.

3.3.1 Response of the cloud fraction to aerosol scenes

Figure 10a shows that the effective cloud fraction increases with increasing τ in cloud free scenes up to 0.09 for $\tau = 1.0$, assuming fine particles ($\alpha = 1.5$), high single scattering albedo ($\omega_0 = 0.95$), $\theta_0 = 25^\circ$ (summer in China) and $\theta = 25^\circ$. Here, aerosols are located between 700 and 800 hPa in the atmosphere (between approximately 2 and 3 km). Similarly to what has been observed in the DOMINO product, the increase of the effective cloud fraction, in the presence of aerosols, is linear and higher with lower surface albedo (i.e. over dark surfaces). In this case, with a surface albedo of 0.07, the effective cloud fraction stays below 0.09 for $\tau = 1.0$, while with a surface albedo of 0.03, the value is close to 0.1. Such an increase is consistent with the impact of the aerosol particles on the continuum reflectance as a function of τ and surface albedo. For these surface albedos and aerosol properties, the scattering effects of aerosols dominate over their extinction.

Figure 10b and c illustrate that aerosol properties (size and absorption) drive the magnitude of the increase of effective cloud fraction. Notably, low α and ω_0 values have smaller impact on the increase of the effective cloud fractions. This illustrates the reduction of scattering effects of aerosols under these conditions. Indeed, low ω_0 values increase the probability of absorption of the photons and so reduce the scattering within the layers and towards the satellite sensor. Coarse particles reduce also the scattering effects by increasing the probability of forward scattering of the photons towards the top of the atmosphere or towards the surface. With fine particles, the ef-

AMTD
8, 8385–8437, 2015

fective cloud fraction varies between 0.06 ($\omega_0 = 0.9$) and more than 0.1 ($\omega_0 = 0.97$) for $\tau = 1.0$.

As a consequence, a higher cloud fraction is understood from the excess TOA reflectance caused by the additional scattering due to aerosols and the impact of the surface reflection. This represents the significant enhanced brightness of the scene (or enhanced scene albedo).

3.3.2 Response of the cloud pressure to aerosol scenes

Figure 11 shows that the retrieved effective cloud pressure decreases with increasing τ (or AOT). This decrease is linked to the O_2-O_2 shielding effect which strongly depends on τ. Such a behavior represents the absorption of the photons by optically thicker aerosol layer, shortening the length of the average light path. At high τ values, the retrieved cloud pressure correlates with the aerosol layer height. Overall, the values are close or smaller than the mean aerosol layer height which may be caused by the model error (i.e. difference between the cloud model and the aerosol spectral effects). At small τ values, the mean aerosol layer height has no effect on the retrieved cloud pressure. The retrieved values stay close to the surface pressure.

Low amount of aerosols have little effects on the O_2-O_2 SCD and the continuum reflectance (and so the effective cloud fraction). The underestimation of the retrieved cloud pressure, in those cases, may be caused by the coarse sampling of the employed LUT. This LUT has been intended for representing the cloud spectral effects and not those of thin aerosol layers. Thus, the sampling may be not high enough in case of low cloud fraction values. Small effective cloud fraction values have limited effects on the average light path and the actual designed LUT is not sensitive enough on small changes on the O_2-O_2 absorption as discussed by (Acarreta et al., 2004). When τ increases, the considered entry in the LUT moves from this undetermined regime to a regime where meaningful cloud pressure value can be interpreted. This can be seen in Fig. 10a–c where the transition between both regimes is located between $\tau = 0.6$ and $\tau = 0.8$ assuming $\theta_0 = 25^\circ$ and $\theta = 25^\circ$. This demonstrates a non-linear behavior

AMTD
8, 8385–8437, 2015

between the cloud pressure retrieval and the AOT. Such behaviour are consistent with the analyses of (Boersma et al., 2011), over southern and eastern US, which show that reduced OMI O_2-O_2 cloud pressure values are observed only with high AOTs. Wang et al. (2015a) found that in general the effective cloud fraction of up to 15 % and cloud top pressure from the surface to 900 hPa from OMI are assigned to the condition of "clear sky with presence of aerosol particles".

The value of τ at which the retrieved cloud pressure starts being sensitive to the aerosol layer height depends mainly on the geometry. Figure 12 shows that for larger θ_0 and θ values (i.e. more than 25°), this transition triggers at smaller τ values (around $\tau = 0.4$). This can be understood as an increased average path length traveled by the photons in the atmosphere and higher retrieved effective cloud fraction values (up to 0.15). The effects of aerosol microphysics properties on the effective cloud pressure retrieval depend mainly on the aerosol amount and the geometry. While smaller α and ω_0 values lead to smaller O_2-O_2 SCDs (cf. Fig. 10b and c), the associated effective cloud pressure is lower only for τ well above 1 in case of small angles ($\theta_0 = 25^\circ$ and $\theta = 25^\circ$). However in case of $\theta_0 = 50^\circ$, or $\theta = 45^\circ$, the retrieved values are smaller between $\tau = 0.6$ and $\tau = 1$. Finally, cases with high surface albedo show smaller retrieved effective cloud pressure. The light path is more affected above bright surfaces as the contribution of surface reflection is more attenuated by the thin aerosol layers. This also highlights that a bias on the assumed surface albedo can perturb the effective cloud pressure retrieval in cases of high aerosol amount. For instance, an overestimated surface albedo (because of scattering aerosol affects) can lead to a reduced effective cloud pressure.

Based on these simulations and retrievals, we can now largely understand the decrease of the effective cloud pressure in summer over China. For one part, it is a consequence of presence of fine aerosol particles (most of MODIS Angstrom coefficients are beyond 1.5). Moreover, the boundary layer is generally deeper in summer due to convective growth. The high cloud pressures for low τ values are largely a retrieval artifact (as discussed above); the lower cloud pressures for higher τ are probably more

AMTD
8, 8385–8437, 2015

realistic as in the regime of high τ there is more sensitivity to the layer height (Fig. 10). In winter, this transition from almost no sensitivity at low τ to more sensitivity to the layer height at high τ results in an almost flat curve, probably because the boundary layer itself is quite shallow. The variability that is seen in Fig. 7 is related to the different effects of surface reflectance and variable viewing angles.

4 Implicit vs. explicit aerosol correction in the tropospheric NO_2 AMF

4.1 Tropospheric NO_2 AMF factor based on effective cloud parameters

The behavior of the OMI cloud algorithms in presence of aerosols, as analysed in Sect. 3.3, has consequences on the computation of the tropospheric NO_2 AMF. Indeed, as effective cloud parameters are sensitive to the presence of aerosols, their properties and their location in the atmosphere, they apply an implicit aerosol correction as observed in the DOMINO product (Sect. 2). This implicit aerosol correction is obtained through the altitude-resolved AMF $a(\Psi, p)$ which uses the retrieved effective cloud fraction and cloud pressure, that are impacted by the presence of aerosols, and no explicit aerosol information. This differs from an explicit aerosol correction where explicit aerosol parameters would be used.

Similarly to Fig. 3, Fig. 13 depicts the resulting tropospheric NO_2 AMF factor f following Eq. (5) at 439 nm, based this time on effective cloud parameters: i.e. the computation of A^{tr} is not based on τ and other aerosol properties, but on effective cloud fraction values between 0. and 0.1 and different cloud pressures. The denominator of f corresponds here to cloud-free cases (i.e. effective cloud fraction = 0). Two surface albedo values are considered (0.05 and 0.07), $\theta_0 = 25^\circ$, $\theta = 25^\circ$ and NO_2 profiles from TM5 in July at 12:00 p.m. (cf. Fig. 1). In case of strong aerosol contamination (i.e. effective cloud fraction = 0.1), the implicit aerosol factor lies in the range of 1.15–0.6: i.e. 15 % enhanced sensitivity if the cloud is retrieved close to the surface and likely well mixed (even below) the tropospheric NO_2 bulk; 40 % reduced sensitivity if the cloud is

AMTD
8, 8385–8437, 2015

retrieved high in the atmosphere. In cases of high τ values, the decrease of effective cloud pressure has more impact on the magnitude of the implicit aerosol than the increase of cloud fraction. Indeed, an increase of effective cloud fraction from 0.08 to 0.1 has an impact of less than 10 %. At the same time, a change of cloud pressure from 900 to 700 hPa can induce a change of 20 % in the AMF factor.

Finally, the variability of the NO_2 profiles causes a higher variability of f, between 10 and 15 %, for cloud pressures between the surface and 700 hPa. It is highly reduced for very high clouds (i.e. cloud pressure between 300 and 500 hpa). This reduction is caused by the absence of scattering properties in the inverse cloud model which results in almost complete masking of the tropospheric NO_2 bulk below the supposed cloud layer. This is contrary to f based on explicit aerosol properties, where even particles with strong shielding effects show a non-negligible sensitivity to the variability of tropospheric NO_2 vertical shape.

Following the sensitivity analyses of the O_2–O_2 cloud retrieval algorithm, the behavior of tropospheric NO_2 AMFs observed in the DOMINO products, over China, can be understood as following: a statistic decrease of tropospheric NO_2 AMF in summer with increasing AOT is caused by the simultaneous increase of effective cloud fraction and decrease of effective cloud pressure. Qualitatively, this behaviour is in line with the expected aerosol shielding effect on tropospheric NO_2 in Summer. Indeed, Vlemmix et al. (2015) has shown that in Summer in China, aerosol particles are generally located above the tropospheric NO_2 layers. The absence of statistic increase/decrease of tropospheric NO_2 AMF in winter with increasing AOT is mainly caused by the smaller effective cloud fraction (compared to Summer) and no variation of effective cloud pressure values which stay close to 900 hPa in average. The accuracy of the implicit aerosol correction is evaluated in the next final sub-section.

AMTD
8, 8385–8437, 2015

4.1.1 Comparison between implicit and explicit aerosol correction on tropospheric NO_2 AMF

The accuracy of the implicit aerosol correction on the tropospheric NO_2, based on the properties of the OMI inverse cloud model and the effective cloud parameters, is discussed through the computation of the relative bias $S_A(\tau)$ in percentage:

$$S_A(\tau) = \frac{A^{tr}(\tau) - A^{tr}_{exp}(\tau)}{A^{tr}_{exp}(\tau)} \cdot 100\,, \tag{8}$$

where $A^{tr}_{exp}(\tau)$ is the tropospheric NO_2 AMF taking explicitly aerosols into account. This relative bias is computed in two ways: (1) assuming that $A^{tr}(\tau)$ includes an implicit aerosol correction (based on the retrieved effective cloud parameters), and (2) that no aerosol correction at all (i.e. $A^{tr}(\tau) = A^{tr}(\tau = 0)$). Then, the actual implicit aerosol correction can be compared to if no aerosol correction was applied (i.e. neither implicit, nor explicit) in the DOMINO product.

Figures 14–16 show that the relative biases S_A induced by the implicit aerosol correction through the effective cloud parameter vary from −10 to 30 % in most of the simulated cases. These biases are negative (i.e. underestimation of the AMFs) and minimal when aerosols are close to the surface and mixed with the tropospheric NO_2 bulk. They are generally positive and maximal (i.e. overestimation of the AMFs) when aerosols are located high in the atmosphere and elevated (i.e. above) compared to the altitude of the tropospheric NO_2 peak, between 950 and 600 hPa depending on the analysed cases. In most of the simulations, the higher bias values are found for scenes with elevated and high aerosol pollution, with $\tau \geq 0.6$. This is a consequence of an insufficient shielding effect applied in the computation of A^{tr} by the implicit aerosol correction through the whole OMI cloud algorithm, resulting from a combination of increased effective cloud fraction value with increasing τ but too large effective cloud pressure values. When the effective cloud pressure value decreases significantly with

AMTD
8, 8385–8437, 2015

increasing AOT, the implicit aerosol correction is then able to reproduce the aerosol shielding effect with a better accuracy. For example, in Fig. 14, when geometry angles are small ($\theta_0 = 25^\circ$ and $\theta = 25^\circ$), with very high aerosol pollution (τ close to 1), fine particles ($\alpha = 1.5$) and high SSA ($\omega_0 \geq 0.95$), the biases S_A decrease from 30 to around 10 %. This decrease is possible as, here, the retrieved effective cloud fraction values are high enough and so the change of O_2–O_2 depth, with respect to the used LUT, can impact the retrieval of effective cloud pressure. In cases of aerosols mixed with NO_2, the biases are likely related to the discrepancy between the opaque Lambertian cloud model and the aerosol properties.

Overall, the relative biases induced by the implicit aerosol correction are generally better than if no aerosol correction was applied in the computation of tropospheric NO_2 AMF. No aerosol correction would induce biases values in the range from −20 to 60 % on A, assuming small geometry angles ($\theta_0 = 25^\circ$ and $\theta = 25^\circ$) and summer NO_2 profiles (cf. Figs. 14 and 15). Assuming winter NO_2 profiles (e.g. Fig. 16a) or larger angles (e.g. $\theta_0 = 50^\circ$ in Fig. 16c), these relative biases can even increase up to 150 % depending on the aerosols altitude. Indeed, in those cases, aerosols apply a stronger shielding effect on the tropospheric NO_2 bulk.

Aerosols altitude and amount (i.e. AOT) are the key drivers of the magnitude of the relative biases S_A. Effects of aerosols microphysic, such as associated SSA or size have a second order of magnitude. Compared to Fig. 14, Fig. 15 shows that coarser particles ($\alpha = 0.5$ instead of 1.5) and reduced SSA (0.9 instead of 0.95) affect mostly the relative biases induced by the implicit aerosol correction for very large AOT ($\tau \geq 1$) by increasing values from around 10 to 40 %. However, these values still remain lower than if no aerosol correction was applied: S_A values close to 55 % in case of high aerosols altitude. For lower AOT values, no significant changes are visible. Figure 16 depicts that the shape of NO_2 vertical profile and large angles do not change significantly the S_A values of implicit aerosol corrections for elevated aerosol layers (from 900 to 600 hPa). Only in the specific case of aerosols located between 900 and 950 hPa, the values are increased (between 50 and 70 %). The cause is an enhancement effect

AMTD
8, 8385–8437, 2015

produced by too large effective cloud pressure while aerosols apply actually a strong shielding effect. Finally, for a given monthly average shape of NO_2 profile, the associated monthly variability induces a variability on the relative biases for implicit aerosol correction between 10 and 20 % (indicated by the error bars on Figs. 14–16). The magnitude of this variability depends on the distance between the aerosols layer and the peak of the tropospheric NO_2 bulk. It is generally larger when the aerosol layers are close to the maximum in the NO_2 profiles.

An overestimation of the tropospheric NO_2 results in an underestimation of the tropospheric NO_2 VCD with the same absolute magnitude according to Eq. (1). The findings identified here on the biases related to the implicit aerosol correction are consistent with those identified in the studies (Shaiganfar et al., 2011; Ma et al., 2013; Kanaya et al., 2014). These studies identified negative biases of around between −26 and −50 % on the OMI tropospheric NO_2 VCD products in regions with high aerosol pollution, in particular in summer. Investigations led by (Ma et al., 2013) show that these underestimations can be explained by the presence of elevated aerosol layers, which are mostly observable in summer in this region (Vlemmix et al., 2015). Very recently, Wang et al. (2015b) analysed MAX-DOAS data over Wuxi city, area with high pollution adjoined to Shangai. It is clearly show that, under aerosol pollution, by using the modified cloud parameters in the collocated DOMINO products, tropospheric NO2 AMFs are overestimated. This mostly happens when the effective cloud pressure value is larger than 900 hPa. Kuhlmann et al. (2015) recalculated tropospheric NO_2 AMFs using high-resolution aerosol parameters over the Pearl River Delta region in southern China by the Models-3 Community Multiscale Air Quality (CMAQ) modelling system. Resulting tropospheric NO_2 VCDs increased by $(+6.0 \pm 8.4)$ %, likely because of polluted cases where the employed aerosol and NO_2 profiles show aerosol particles located higher in altitude compared to tropospheric NO_2. In addition, (Lin et al., 2014), by explicitly taking into account aerosol optical effects from the GEOS-Chem simulations, show that, in average, excluding both aerosol scattering and absorption lead to changes between −40 and 90 % with AOD ≥ 0.8. Castellanos et al. (2015) have reduced the OMI NO_2

AMTD
8, 8385–8437, 2015

VCDs by 10 % in average by using aerosol extinction vertical profile observations from the CALIOP instrument and AOD and SSA from the OMAERUV database for scenes over South-America including absorbing biomass burning aerosols. According to the figures of CALIOP and collocated TM4 NO_2 profiles, the processed cases seem to include aerosol particles mixed (in parts) with the tropospheric NO_2 bulk. Finally, the new POMINO dataset which take aerosol properties from GEOS-Chem simulations, and are based on the reprocessing of all the DOMINO product, show in average a reduction of the tropospheric NO_2 VCDs by 0–40 % over most of China (Lin et al., 2015). However, it is mentioned that individual reductions or enhancements depend strongly on location and season, and thus on the occurence of the relative altitude between aerosol particles and tropospheric NO_2. Overall, all these references which performed real retrievals show consistent numbers and conclusions with the sensitivity study performed here, and highlight the crucial role played by the actual OMI cloud algorithm and the derived implicit aerosol correction. This emphasizes that high aerosol pollution has currently large impacts on the individual OMI tropospheric NO_2 products over industrialised regions and cloud-free scenes.

Relative biases associated with implicit aerosol correction shows an irregular behavior with respect to increasing AOT values. This differs from the smooth increase of relative biases assuming no aerosol correction with respect to AOT. This irregular behaviour probably results from the combination of retrieved effective cloud fraction and pressure, and its complex relation with aerosol amount. This is probably caused by the coarse sampling of the designed cloud LUT. A higher sampling should be designed and tested through the OMI cloud algorithm over scenes dominated by aerosols. The behavior of these biases could lead to complex spatial and temporal patterns of the individual DOMINO tropospheric NO_2 products over highly polluted areas, not consistent with the physical NO_2 and aerosol patterns. The potential impacts on the estimation of NO_x surface fluxes should be investigated.

AMTD
8, 8385–8437, 2015

5 Conclusions

In this paper, the behavior of the OMI cloud model for cloud-free scenes with aerosols present was studied as well as the accuracy of the cloud-model based aerosol correction of tropospheric NO_2 AMFs. This study focused on the operational OMI DOMINO product for cloud-free scenes, its behavior in the presence of aerosol dominated scenes that were selected based on collocated MODIS Aqua aerosol products, and the comparison with numerical simulated study cases. The goals were to understand the behavior of the implicit aerosol correction based on the OMI cloud retrieval, and to investigate how much it improves the accuracy of the tropospheric NO_2 AMFs compared to performing no correction (and assuming clear sky conditions with no aerosols). Analyses relied on a model vs. observation approach and have focused specifically on the industrialized part of East China.

The OMI cloud algorithm cannot distinguish aerosol and cloud signals. Effective cloud parameters are retrieved over cloud-free scenes but including aerosol particles. This implies that these retrievals include considerable aerosol information (AOT, optical properties, particles size, altitude) but they are treated as an opaque Lambertian reflector (albedo of 0.8). The effective cloud fraction increases linearly with increasing AOT and can reach values between 0.1 and 0.15 for AOT = 1. This represents the aerosol scattering effects on the 460–490 nm continuum reflectance. The slope of the linear regression of AOT vs cloud is, however, dependent on the aerosol properties, the surface albedo and the SZA and VZA. The response of effective cloud pressure to aerosol scenes represents the O_2–O_2 shielding effect induced by the absorption of photons by optically thicker aerosol layers, shortening the length of the average light path. In case of high aerosol pollution, retrieved effective cloud pressure values correlate with the mean aerosol layer height. Values smaller than the mean aerosol layer pressure may be related to the cloud model error used over aerosol scenes. In cases of low AOT or effective cloud fraction values, aerosols have little effect on O_2–O_2 absorption, leading to effective cloud pressure values close to the surface pressure independently of the al-

AMTD
8, 8385–8437, 2015

titude of the aerosol layer. This overestimation can be caused by the coarse sampling of the cloud LUT used by the OMI cloud algorithm to convert the O_2–O_2 continuum reflectance and slant column into effective cloud fraction and pressure. Indeed, this LUT was initially intended for retrievals over cloudy scenes, not for cloud-free scenes dominated by aerosols.

Aerosols can either decrease (shielding) or increase (enhancement) the sensitivity to tropospheric NO_2 bulk. Such effects depend simultaneously on the aerosols altitude and the shape of the NO_2 vertical profile. Shielding effects occur mostly when particles are above the NO_2 layers which should happen mostly during summer in China. Generally, if no aerosol correction was performed in the DOMINO products, relative biases of the tropospheric NO_2 VCDs would range from −60 to 20 % for large AOT values. These values could even decrease to −150 % in cases of large angles (e.g. SZA $\geq 50^{\circ}$) or very large vertical separation between aerosols and the tropospheric NO_2 bulk.

An implicit aerosol correction is actually applied in the computation of the tropospheric NO_2 AMF through the use of the retrieved effective cloud fraction and pressure over scenes dominated by aerosols. After the implicit aerosol correction, relative biases in the VCDs are negative and in the range of −40 to −20 % remain in case of elevated aerosol particles and high pollution (AOT ≥ 0.6). In case of aerosols located close to the surface or mixed with the tropospehric NO_2 bulk, relative biases in the VCDs are positive and in the range of 10 to 20 %. These values are smaller than if no aerosol correction was applied in the OMI DOMINO products. AOTs and aerosols altitude are the key drivers of these biases, while aerosol microphysical properties are of secondary importance. Note that geometry angles and shape of the NO_2 profile can either increase or decrease these values. For elevated aerosols, the main cause of these biases is an underestimation of the aerosol shielding effect by the cloud algorithm. The reason of this underestimation is probably a combination of the cloud model error, used in presence of aerosols, and the employed numerical approach to convert the O_2–O_2 continuum reflectance and SCD into effective cloud fraction and pressure

AMTD
8, 8385–8437, 2015

through a LUT. Furthermore, the coarse sampling in the employed cloud LUT leads to complex behaviors between these biases and AOT. An improved LUT with a higher sampling should be implemented and evaluated. The impact on the ability to estimate the NO_x surface fluxes should be further studied. The biases in presence of aerosols located to the surface or mixed with tropospheric NO_2 are likely a consequence of difference between the opaque Lambertian cloud model and aerosol properties.

The present analyses consider box aerosol layers (i.e. discrete atmospheric layers with constant aerosol extinction value) and assume that aerosols cover completely the OMI pixels. It is recognized that a more realistic description of the vertical distribution of aerosols and assumptions of OMI pixels partially covered by aerosols would result in different biases. Nevertheless, biases found here compare quite well to biases found in various ground-based comparison studies. Finally, all the sensitivity studies performed here assume that, in case of highly polluted regions, only non-explicit aerosol correction impact the current individual OMI tropospheric NO_2 products. It should be noted that uncertainties in the shape of vertical NO_2 profile and climatology surface albedo can also play significant role on the estimated biases when aerosols are present in the measurement.

The results described in this paper indicate that it is worthwhile to design and evaluate an improved aerosol correction in view of retrieving tropospheric NO_2 vertical column densities. This is needed in the context of OMI measurements, but even more in the future for TROPOMI (Veefkind et al., 2012). Since the spatial resolution will be higher (7 km × 7 km), there is a significant probability that a scene will be fully covered by aerosol particles.

Acknowledgements. This work was funded by the Netherlands Space Office (NSO) under the OMI contract. The authors thank Maarten Sneep for sharing his experience with respect to the use of DISAMAR software. We are grateful to Folkert Boersma for the exchanges on understanding the NO_2 and cloud products and his helpful comments related to this work. We thank also Twan von Noije and Michiel van Weele for proving the TM5 data.

AMTD
8, 8385–8437, 2015

References

Acarreta, J. R., De Haan, J. F., and Stammes, P.: Cloud pressure retrieval using the O_2–O_2 absorption band at 477 nm, J. Geophys. Res., 109, D05204, doi:10.1029/2003JD003915, 2004. 8388, 8399, 8400, 8402

Boersma, K. F., Eskes, H. J., and Brinksma, E. J.: Error analysis for tropospheric NO_2 retrieval from space, J. Geophys. Res., 109, D04311, doi:10.1029/2003JD003962, 2004. 8387, 8389

Boersma, K. F., Eskes, H. J., Veefkind, J. P., Brinksma, E. J., van der A, R. J., Sneep, M., van den Oord, G. H. J., Levelt, P. F., Stammes, P., Gleason, J. F., and Bucsela, E. J.: Near-real time retrieval of tropospheric NO_2 from OMI, Atmos. Chem. Phys., 7, 2103–2118, doi:10.5194/acp-7-2103-2007, 2007. 8388

Boersma, K. F., Eskes, H. J., Dirksen, R. J., van der A, R. J., Veefkind, J. P., Stammes, P., Huijnen, V., Kleipool, Q. L., Sneep, M., Claas, J., Leitão, J., Richter, A., Zhou, Y., and Brunner, D.: An improved tropospheric NO_2 column retrieval algorithm for the Ozone Monitoring Instrument, Atmos. Meas. Tech., 4, 1905–1928, doi:10.5194/amt-4-1905-2011, 2011. 8388, 8389, 8390, 8392, 8403

Bovensman, H., Burrows, J. P., Buchwitz, M., Frerick, J., Noel, S., Rozanov, V. V., Chance, K. V., and Goede, A. P. H.: SCIAMACHY: mission objectives and measurement modes, J. Atmos. Sci., 56, 127–150, 1999. 8387

Burrows, J. P., Weber, M., Buchwitz, M., Rozanov, V. V., Ladstädter-Weissenmayer, A., Richter, A., de Beek, R., Hoogen, R., Bramstedt, K., Eichmann, K.-U., Eisinger, M., and Perner, D.: The Global Ozone Monitoring Experiment (GOME): mission concept and first scientific results, J. Atmos. Sci., 56, 151–175, 1999. 8387

Castellanos, P., Boersma, K. F., Torres, O., and de Haan, J. F.: OMI tropospheric NO_2 air mass factors over South America: effects of biomass burning aerosols, Atmos. Meas. Tech. Discuss., 8, 2683–2733, doi:10.5194/amtd-8-2683-2015, 2015. 8389, 8408

Curier, R. L., Kranenburg, R., Segers, A. J. S., Timmermans, R. M. A., and Schaap, M.: Synergistic use of OMI NO_2 tropospheric columns and LOTOS-EUROS to evaluate the NO_x emission trends across Europe, Remote Sens. Environ., 149, 58–69, doi:10.1016/j.rse.2014.03.032, 2014. 8388

De Haan, J. F., Bosma, P. B., and Hovenier, J. W.: The adding method for multiple scattering calculations of polarized light, Astron. Astrophys., 183, 371–391, 1987. 8393

AMTD
8, 8385–8437, 2015

De Haan, J. F.: DISAMAR Algorithm Description and Background Information, Royal Netherlands Meteoroligical Institute, De Bilt, the Netherlands, 2011. 8393

Dirksen, R. J., Folkert Boersma, K., de Laat, J., Stammes, P., van der Werf, G. R., Val Martin, M., and Kelder, H. M.: An aerosol boomerang: Rapid around-the-world transport of smoke from the December 2006 Australian forest fires observed from space, J. Geophys. Res., 114, D21201, doi:10.1029/2009JD012360, 2009.

Hendrick, F., Müller, J.-F., Clémer, K., Wang, P., De Mazière, M., Fayt, C., Gielen, C., Hermans, C., Ma, J. Z., Pinardi, G., Stavrakou, T., Vlemmix, T., and Van Roozendael, M.: Four years of ground-based MAX-DOAS observations of HONO and NO_2 in the Beijing area, Atmos. Chem. Phys., 14, 765–781, doi:10.5194/acp-14-765-2014, 2014.

Hovenier, J. W. and Hage, J. I.: Relations involving the spherical albedo and other photometric quantities of planets with atmospheres, Astron. Astrophys., 214, 391–401, 1989. 8393

Huijnen, V., Eskes, H. J., Poupkou, A., Elbern, H., Boersma, K. F., Foret, G., Sofiev, M., Valdebenito, A., Flemming, J., Stein, O., Gross, A., Robertson, L., D'Isidoro, M., Kioutsioukis, I., Friese, E., Amstrup, B., Bergstrom, R., Strunk, A., Vira, J., Zyryanov, D., Maurizi, A., Melas, D., Peuch, V.-H., and Zerefos, C.: Comparison of OMI NO_2 tropospheric columns with an ensemble of global and European regional air quality models, Atmos. Chem. Phys., 10, 3273–3296, doi:10.5194/acp-10-3273-2010, 2010.

Jacob, D. J., Heikes, B. G, Fan, S.-M., Logan, J. A., Mauzerall, D. L., Bradshaw, J. D., Singh, H. B., Gregory, G. L., Talbot, R. W., Blake, D. R., Sachse, G. W.: Origin of ozone and NO_x in the tropical troposphere: a photochemical analysis of aircraft observations over the South Atlantic basin, J. Geophys. Res., 101, 24235–24250, 1996. 8387

Kanaya, Y., Irie, H., Takashima, H., Iwabuchi, H., Akimoto, H., Sudo, K., Gu, M., Chong, J., Kim, Y. J., Lee, H., Li, A., Si, F., Xu, J., Xie, P.-H., Liu, W.-Q., Dzhola, A., Postylyakov, O., Ivanov, V., Grechko, E., Terpugova, S., and Panchenko, M.: Long-term MAX-DOAS network observations of NO_2 in Russia and Asia (MADRAS) during the period 2007–2012: instrumentation, elucidation of climatology, and comparisons with OMI satellite observations and global model simulations, Atmos. Chem. Phys., 14, 7909–7927, doi:10.5194/acp-14-7909-2014, 2014. 8388, 8408

King, M. D., Kaufman, Y. J., Menzel, W. P., and Tanre, D.: Remote sensing of cloud, aerosol, and water vapor properties from the Moderate Resolution Imaging Spectrometer (MODIS), IEEE T. Geosci. Remote, 30, 2–27, 1992.

AMTD
8, 8385–8437, 2015

Kleipool, Q. L., Dobber, M. R., de Haan, J. F., and Levelt, P. F.: Earth surface reflectance climatology from 3 years of OMI data, J. Geophys. Res., 113, D18308, doi:10.1029/2008JD010290, 2008. 8398, 8427

Kuhlmann, G., Lam, Y. F., Cheung, H. M., Hartl, A., Fung, J. C. H., Chan, P. W., and Wenig, M. O.: Development of a custom OMI NO_2 data product for evaluating biases in a regional chemistry transport model, Atmos. Chem. Phys., 15, 5627–5644, doi:10.5194/acp-15-5627-2015, 2015. 8408

Lamsal, L. N., Krotkov, N. A., Celarier, E. A., Swartz, W. H., Pickering, K. E., Bucsela, E. J., Gleason, J. F., Martin, R. V., Philip, S., Irie, H., Cede, A., Herman, J., Weinheimer, A., Szykman, J. J., and Knepp, T. N.: Evaluation of OMI operational standard NO_2 column retrievals using in situ and surface-based NO_2 observations, Atmos. Chem. Phys., 14, 11587–11609, doi:10.5194/acp-14-11587-2014, 2014. 8388

Leitão, J., Richter, A., Vrekoussis, M., Kokhanovsky, A., Zhang, Q. J., Beekmann, M., and Burrows, J. P.: On the improvement of NO_2 satellite retrievals – aerosol impact on the airmass factors, Atmos. Meas. Tech., 3, 475–493, doi:10.5194/amt-3-475-2010, 2010. 8388, 8389, 8392

Levelt, P. F., Hilsenrath, E., Leppelmeier, G. W., van den Oord, G. H. J., Bhartia, P. K., Tamminen, J., de Haan, J. F., and Veefkind, J. P.: Science objectives of the Ozone Monitoring Instrument, IEEE T. Geosci. Remote, 44, 1199–1208, doi:10.1109/TGRS.2006.872336, 2006. 8387

Lin, J.-T., Martin, R. V., Boersma, K. F., Sneep, M., Stammes, P., Spurr, R., Wang, P., Van Roozendael, M., Clémer, K., and Irie, H.: Retrieving tropospheric nitrogen dioxide from the Ozone Monitoring Instrument: effects of aerosols, surface reflectance anisotropy, and vertical profile of nitrogen dioxide, Atmos. Chem. Phys., 14, 1441–1461, doi:10.5194/acp-14-1441-2014, 2014. 8388, 8389, 8408

Lin, J.-T., Liu, M.-Y., Xin, J.-Y., Boersma, K. F., Spurr, R., Martin, R., and Zhang, Q.: Influence of aerosols and surface reflectance on satellite NO_2 retrieval: seasonal and spatial characteristics and implications for NO_x emission constraints, Atmos. Chem. Phys. Discuss., 15, 12653–12714, doi:10.5194/acpd-15-12653-2015, 2015. 8409

Ma, J. Z., Beirle, S., Jin, J. L., Shaiganfar, R., Yan, P., and Wagner, T.: Tropospheric NO_2 vertical column densities over Beijing: results of the first three years of ground-based MAX-DOAS measurements (2008–2011) and satellite validation, Atmos. Chem. Phys., 13, 1547–1567, doi:10.5194/acp-13-1547-2013, 2013. 8388, 8408

AMTD
8, 8385–8437, 2015

Määttä, A., Laine, M., Tamminen, J., and Veefkind, J. P.: Quantification of uncertainty in aerosol optical thickness retrieval arising from aerosol microphysical model and other sources, applied to Ozone Monitoring Instrument (OMI) measurements, Atmos. Meas. Tech., 7, 1185–1199, doi:10.5194/amt-7-1185-2014, 2014.

Platt, U. and Stutz, J.: Differential Optical Absorption Spectroscopy (DOAS), Principles and Applications, Springer, Berlin-Heidelberg, Germany, doi:10.1007/978-3-540-75776-4, 2008. 8390

Remer, L. A., Kleidman, R. G., Levy, R. C., Kaufman, Y. J., Tanre, D., Mattoo, S., Martins, J. V., Ichoku, C., Koren, I., Yu, H., and Holben, B. N.: Global aerosol climatology from the MODIS satellite sensors, J. Geophys. Res., 113, D14S07, doi:10.1029/2007JD009661, 2008. 8397

Reuter, M., Buchwitz, M., Hilboll, A., Richter, A., Schneising, O., Hilker, M., Heymann, J., Bovensmann, H., and Burrows, J. P.: Decreasing emissions of NO_x relative to CO_2 in East Asia inferred from satellite observations, Nat. Geosci. Lett., 7, 792–795, doi:10.1038/NGEO2257, 2014. 8388

Rozanov, V. V. and Rozanov, A. V.: Differential optical absorption spectroscopy (DOAS) and air mass factor concept for a multiply scattering vertically inhomogeneous medium: theoretical consideration, Atmos. Meas. Tech., 3, 751–780, doi:10.5194/amt-3-751-2010, 2010. 8391

Shaiganfar, R., Beirle, S., Sharma, M., Chauhan, A., Singh, R. P., and Wagner, T.: Estimation of NO_x emissions from Delhi using Car MAX-DOAS observations and comparison with OMI satellite data, Atmos. Chem. Phys., 11, 10871–10887, doi:10.5194/acp-11-10871-2011, 2011. 8388, 8408

Shindell, D. T., Faluvegi, G., Koch, D. M., Schmidt, G. A., Unger, N., and Bauer, S. E.: Improved attribution of climate forcing to emissions, Science, 326, 716–718, 2009. 8387

Sneep, M., de Haan, J. F., Stammes, P., Wang, P., Vanbauce, C., Joiner, J., Vasilkov, A. P., and Levelt, P. F.: Three-way comparison between OMI and PARASOL cloud pressure products, J. Geophys. Res., 113, D15S23, doi:10.1029/2007JD008694, 2008. 8399

Stammes, P.: Spectral radiance modelling in the UV–Visible range, in: IRS 2000: Current Problems in Atmospheric Radiation, edited by: Smith, W. L. and Timofeyev Y. M., A. Deepak, Hampton, VA, USA, 385–388, 2001. 8393

Stammes, P., Sneep, M., de Haan, J. F., Veefkind, J. P., Wang, P., and Levelt, P. F.: Effective cloud fractions from the Ozone Monitoring Instrument: theoretical framework and validation, J. Geophys. Res., 113, D16S38, doi:10.1029/2007JD008820, 2008. 8399

AMTD
8, 8385–8437, 2015

Valks, P., Pinardi, G., Richter, A., Lambert, J.-C., Hao, N., Loyola, D., Van Roozendael, M., and Emmadi, S.: Operational total and tropospheric NO_2 column retrieval for GOME-2, Atmos. Meas. Tech., 4, 1491–1514, doi:10.5194/amt-4-1491-2011, 2011. 8388

van Noije, T. P. C., Le Sager, P., Segers, A. J., van Velthoven, P. F. J., Krol, M. C., Hazeleger, W., Williams, A. G., and Chambers, S. D.: Simulation of tropospheric chemistry and aerosols with the climate model EC-Earth, Geosci. Model Dev., 7, 2435–2475, doi:10.5194/gmd-7-2435-2014, 2014. 8394, 8420

Veefkind, J. P., Boersma, K. F., Wang, J., Kurosu, T. P., Krotkov, N., Chance, K., and Levelt, P. F.: Global satellite analysis of the relation between aerosols and short-lived trace gases, Atmos. Chem. Phys., 11, 1255–1267, doi:10.5194/acp-11-1255-2011, 2011. 8388

Veefkind, J. P., Aben, I., McMullan, K., Förster, H., de Vries, J., Otter, G., Claas, J., Eskes, H. J., de Haan, J. F., Kleipool, Q., van Weele, M., Hasekamp, O., Hoogeveen, R., Landgraf, J., Snel, R., Tol, P., Ingmann, P., Voors, R., Kruizinga, B., Vink, R., Visser, H., and Levelt, P.: TROPOMI on the ESA Sentinel-5 Precursor: a GMES mission for global observations of the atmospheric composition for climate, air quality and ozone layer applications, Remote Sens. Environ., 120, 70–83, doi:10.1016/j.rse.2011.09.027, 2012. 8412

Vlemmix, T., Hendrick, F., Pinardi, G., De Smedt, I., Fayt, C., Hermans, C., Piters, A., Wang, P., Levelt, P., and Van Roozendael, M.: MAX-DOAS observations of aerosols, formaldehyde and nitrogen dioxide in the Beijing area: comparison of two profile retrieval approaches, Atmos. Meas. Tech., 8, 941–963, doi:10.5194/amt-8-941-2015, 2015. 8405, 8408

Wagner, T., Burrows, J. P., Deutschmann, T., Dix, B., von Friedeburg, C., Frieß, U., Hendrick, F., Heue, K.-P., Irie, H., Iwabuchi, H., Kanaya, Y., Keller, J., McLinden, C. A., Oetjen, H., Palazzi, E., Petritoli, A., Platt, U., Postylyakov, O., Pukite, J., Richter, A., van Roozendael, M., Rozanov, A., Rozanov, V., Sinreich, R., Sanghavi, S., and Wittrock, F.: Comparison of box-air-mass-factors and radiances for Multiple-Axis Differential Optical Absorption Spectroscopy (MAX-DOAS) geometries calculated from different UV/visible radiative transfer models, Atmos. Chem. Phys., 7, 1809–1833, doi:10.5194/acp-7-1809-2007, 2007. 8391

Wang, P., Tuinder, O. N. E., Tilstra, L. G., de Graaf, M., and Stammes, P.: Interpretation of FRESCO cloud retrievals in case of absorbing aerosol events, Atmos. Chem. Phys., 12, 9057–9077, doi:10.5194/acp-12-9057-2012, 2012.

Wang, Y., Penning de Vries, M., Xie, P. H., Beirle, S., Dörner, S., Remmers, J., Li, A., and Wagner, T.: Cloud and aerosol classification for 2 1/2 years of MAX-DOAS observations in

AMTD
8, 8385–8437, 2015

Wuxi (China) and comparison to independent data sets, Atmos. Meas. Tech. Discuss., 8, 4653–4709, doi:10.5194/amtd-8-4653-2015, 2015a. 8389, 8403

Wang, Y., Wagner, T., Xie, P., Li, A., Beirle, S., Theys, N., Stavrakou, T., De Smedt, I., and Koukouli, M.: MAX-DOAS observations and their application to the validation of satellite and model data in Wuxi, China, 7th DOAS workshop 2015, Brussels, Belgium, 7 July 2015, doi:10.13140/RG.2.1.2379.6325, 2015b. 8388, 8408

AMTD

8, 8385–8437, 2015

Table 1. List of the physical variables (Ψ) requested for the computation of the tropospheric NO_2 AMF, through the altitude-resolved AMF $a(p^*)$. For each of these variables, an indication about its degree of certainty is given.

Ψ	Degree of certainty
SZA (θ_0)	High
VZA (θ)	High
Relative azimuth angle ($\phi - \phi_0$)	High
Wavelength	High
Surface pressure	High
Surface albedo	Moderate
Vertical temperature profile	Moderate
Vertical pressure profile	Moderate
Cloud parameters	Moderate (see Sect. 3 for further details)
Aerosol properties	Low (see Sect. 2 for further details)
Vertical NO_2 profile	Low

AMTD
8, 8385–8437, 2015

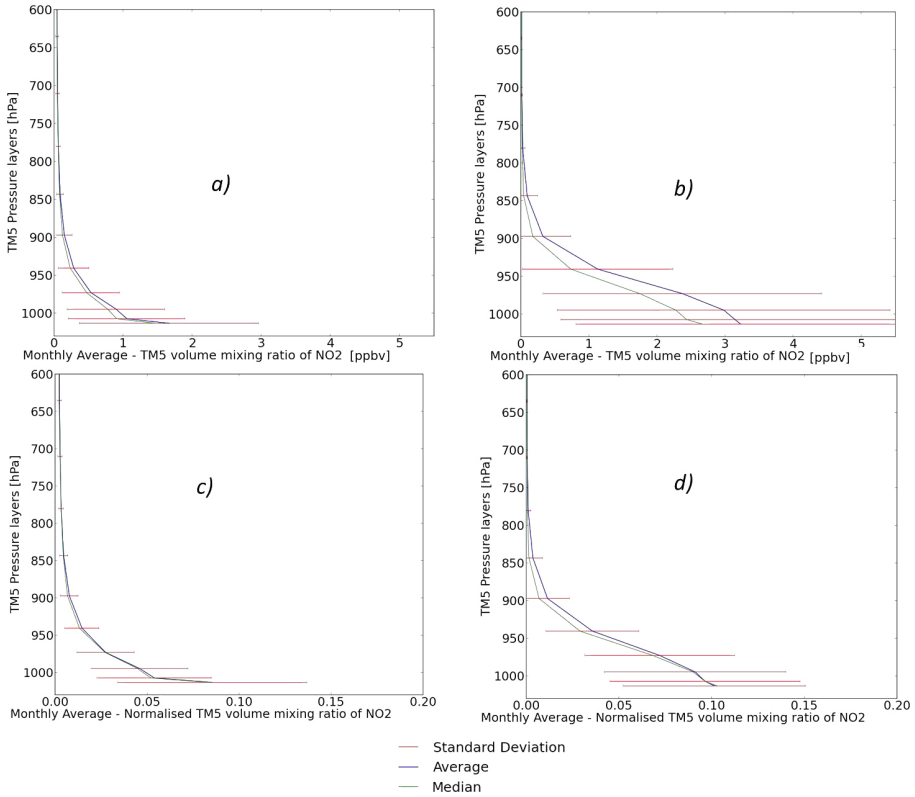

Figure 1. Monthly average NO_2 vertical profiles at 12:00 from TM5 simulations, 2006, East China (van Noije et al., 2014). **(a)** VMR tropospheric NO_2 profile in July, **(b)** VMR tropospheric NO_2 profile in January, **(c)** normalised tropospheric NO_2 profile in July, **(d)** normalised tropospheric NO_2 profile in January. Normalisations are done by dividing the VMR of each atmospheric layer to the total column integrated along the atmospheric layers.

AMTD
8, 8385–8437, 2015

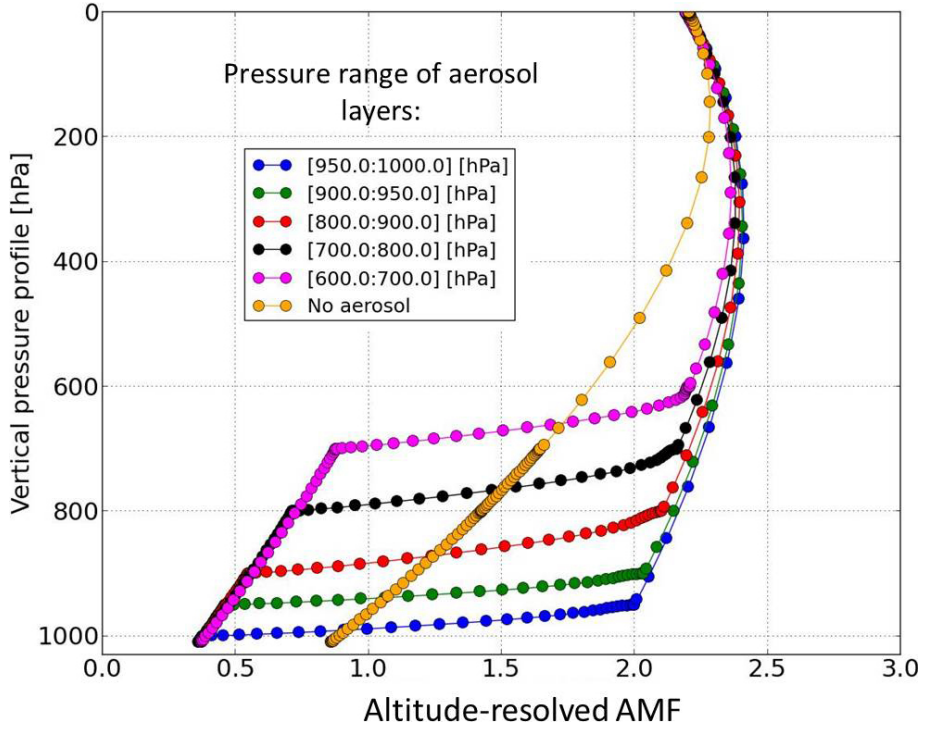

Figure 2. Altitude-resolved AMF at 439 nm as computed by DISAMAR for surface albedo = 0.05, SZA = 25°, VZA = 25°. Computations are done without and with aerosols at different layers. Aerosols are specified with AOT = 1, SSA = 0.95, Angstrom coefficient = 1.5 and assymetry parameter 0.7.

AMTD
8, 8385–8437, 2015

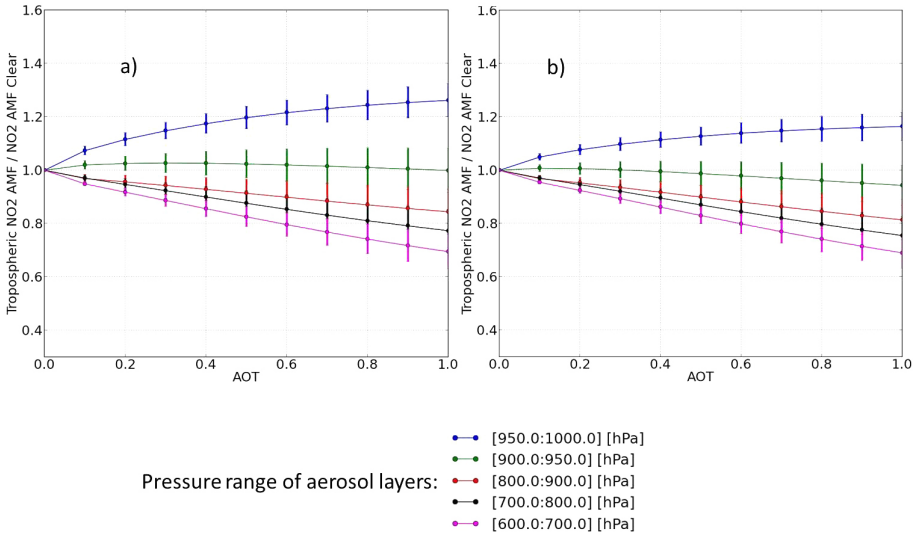

Figure 3. Ratio (f) of AMFs at 439 nm (cf. Eq. 5) as a function of AOT for surface albedo = 0.05 **(a)** and 0.07 **(b)**. f is determined for all the NO_2 vertical profiles from TM5 simulations over 2006, East China, July 2006 (cf. Fig. 1), SZA = 25°, VZA = 25°, aerosol Angstrom coefficient = 1.5, SSA = 0.95, asymmetry parameter = 0.7 for the Henyey–Greenstein phase function. The curves connect the average values per AOT bin and the error bars represent the standard deviation, of f computed for all the individual TM5 NO_2 profiles over this period and this region.

AMTD
8, 8385–8437, 2015

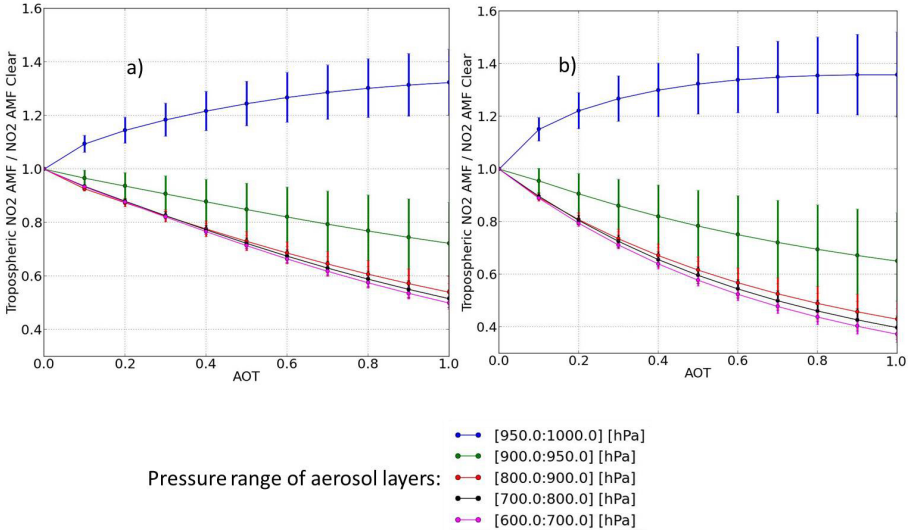

Figure 4. (a) Similar as Fig. 3a, but with NO_2 profiles for January. **(b)** Similar as Fig. 4a, but with SZA = 50°.

AMTD
8, 8385–8437, 2015

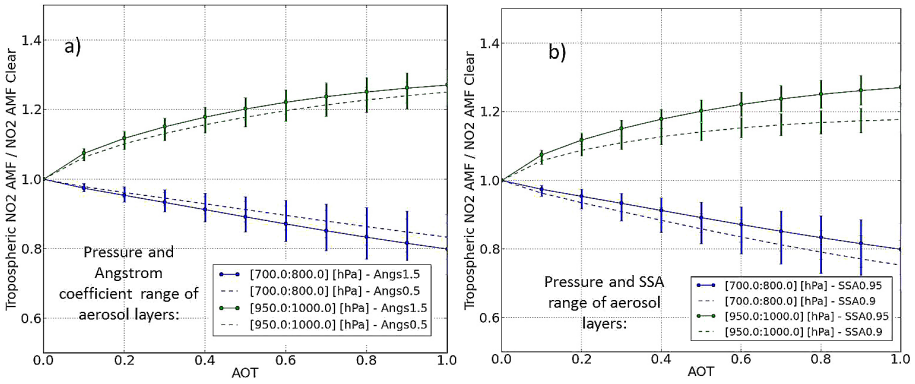

Figure 5. Similar as Fig. 3, but with only 2 different atmospheric aerosol layers: **(a)** 2 Angstrom coefficient values: 1.5 (fine particles) and 0.5 (coarse particles), **(b)** 2 SSA values: 0.95 and 0.5.

AMTD
8, 8385–8437, 2015

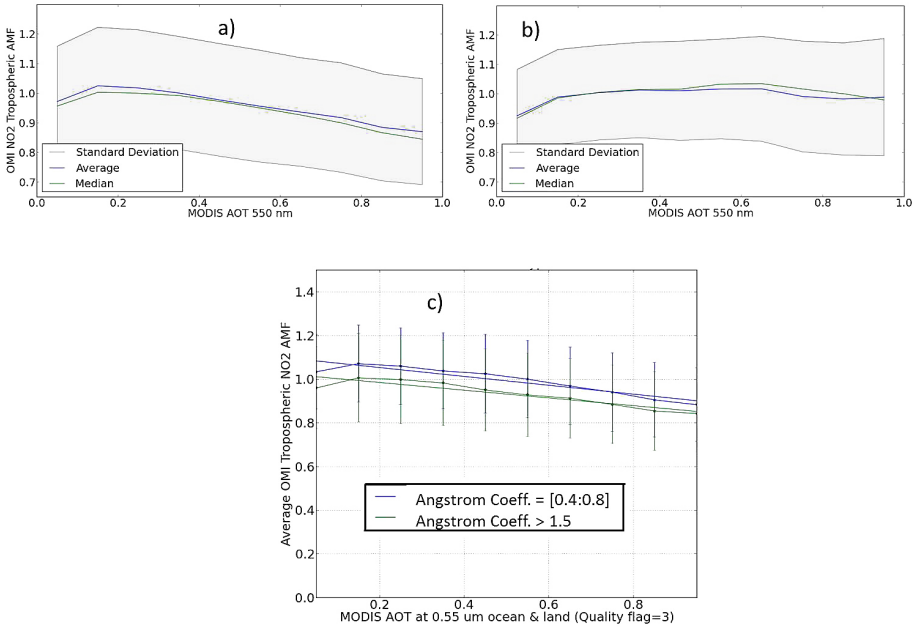

Figure 6. Tropospheric NO_2 AMFs from the OMI DOMINO v2 plotted against MODIS Aqua AOT. Statistics computed over 3 years (2005, 2006, 2007) and following the methodology described in Sect. 3: **(a)** summer (June, July, August), **(b)** winter (December, January, February), over East China, **(c)** summer, distinction between 2 ranges of MODIS Aqua aerosols Angstrom coefficient.

AMTD
8, 8385–8437, 2015

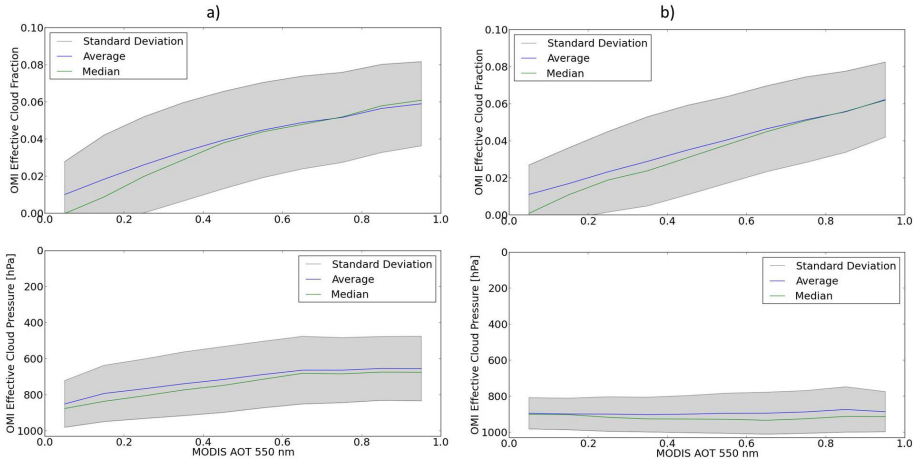

Figure 7. Effective cloud fraction and cloud pressure extracted from OMI DOMINO v2 compared to MODIS Aqua AOT for 2 seasons. Statistics are computed over 3 years (2005, 2006, 2007) and following the methodology described in Sect. 3.1: **(a)** summer (June, July, August), **(b)** winter (December, January, February) over East China.

AMTD
8, 8385–8437, 2015

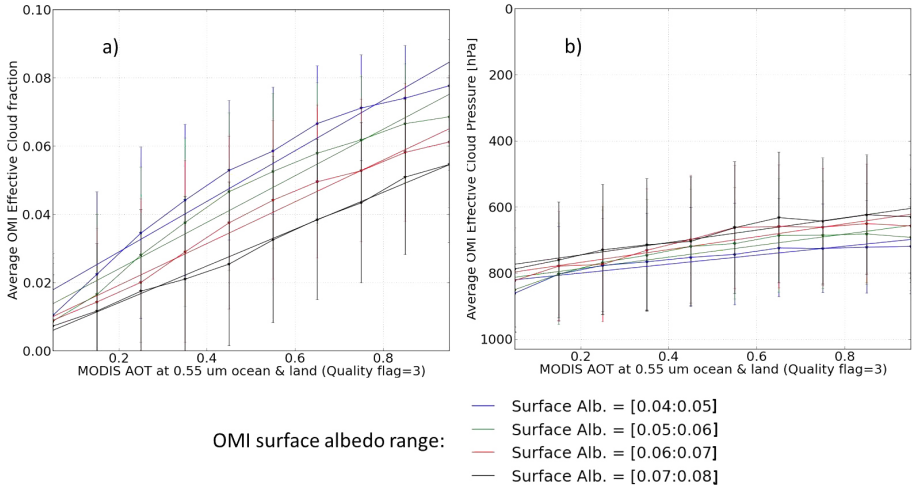

Figure 8. OMI effective cloud parameters extracted from OMI DOMINO v2 compared to MODIS Aqua AOT, as a function of the OMI climatology surface albedo (Kleipool et al., 2008). Statistics computed over 3 years (2005, 2006, 2007), summer (June, July, August) over East China (cf. Sect. 3.1): **(a)** effective cloud fraction, **(b)** effective cloud pressure.

AMTD
8, 8385–8437, 2015

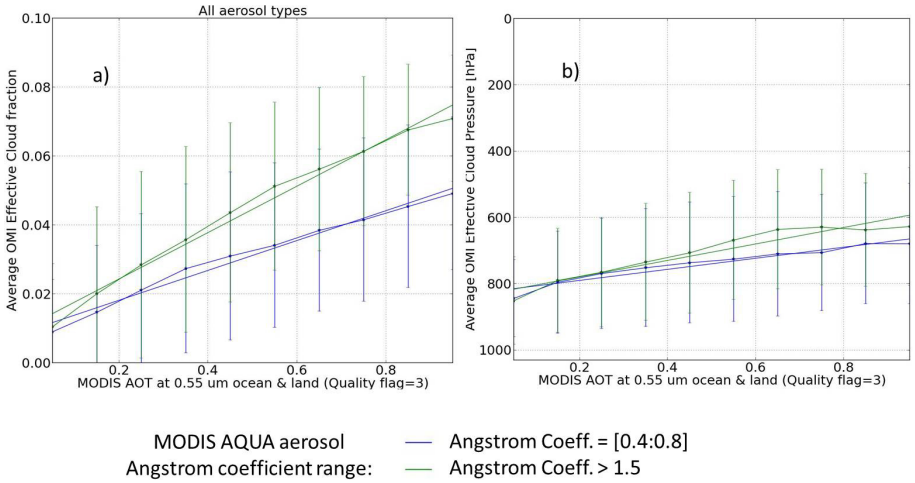

Figure 9. Similar as Fig. 8 but as a function of the MODIS aerosol angstrom coefficient: **(a)** effective cloud fraction, **(b)** effective cloud pressure.

AMTD
8, 8385–8437, 2015

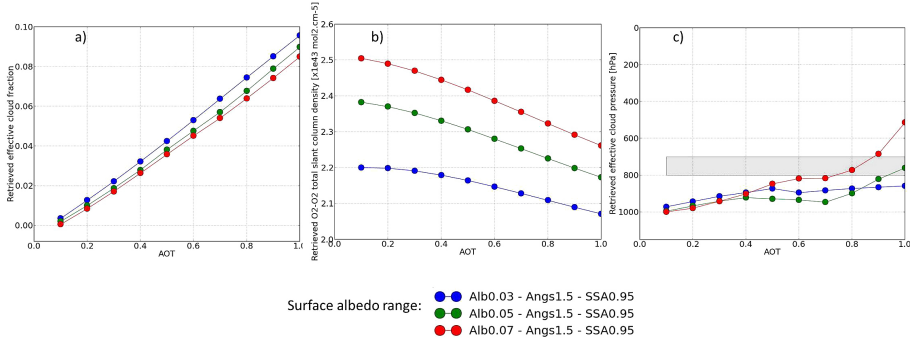

Figure 10a. Simulated DOAS O_2-O_2 cloud retrieval results, based on noise-free spectra with aerosols, as a function of AOT and surface albedo, assuming an opaque (albedo = 0.8) Lambertian cloud forward model. The results are derived from the following geophysical conditions: average of temperature, H_2O, O_3, and NO_2 vertical profiles from TM5 month July (see Fig. 1), O_3 total column = 250 DU, SZA = 25° and VZA = 25°, surface pressure = 1010 hPa. Aerosol properties are: SSA = 0.95, Angstrom coefficient = 1.5 (fine particles), asymmetry parameter = 0.7, layers located between 700 and 800 hPa: **(a)** effective cloud fraction, **(b)** O_2-O_2 total slant column density, **(c)** effective cloud pressure (grey colour depicts the location of the simulated aerosol layers).

AMTD
8, 8385–8437, 2015

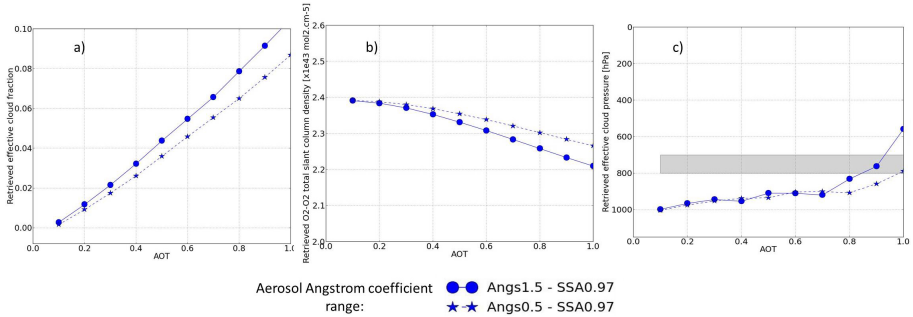

Figure 10b. As Fig. 10a but the results are depicted as a function of Aerosols AOT and Angstrom coefficient. The surface albedo is here constant (0.05).

AMTD
8, 8385–8437, 2015

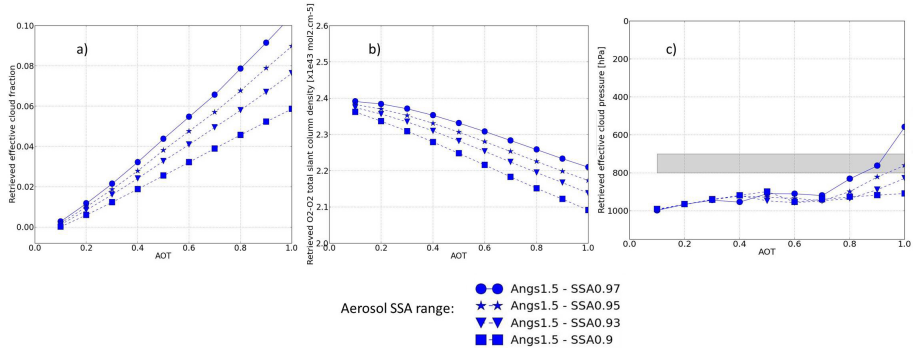

Figure 10c. As Fig. 10a but the results are depicted as a function of Aerosols AOT and SSA. The surface albedo is here constant (0.05).

AMTD
8, 8385–8437, 2015

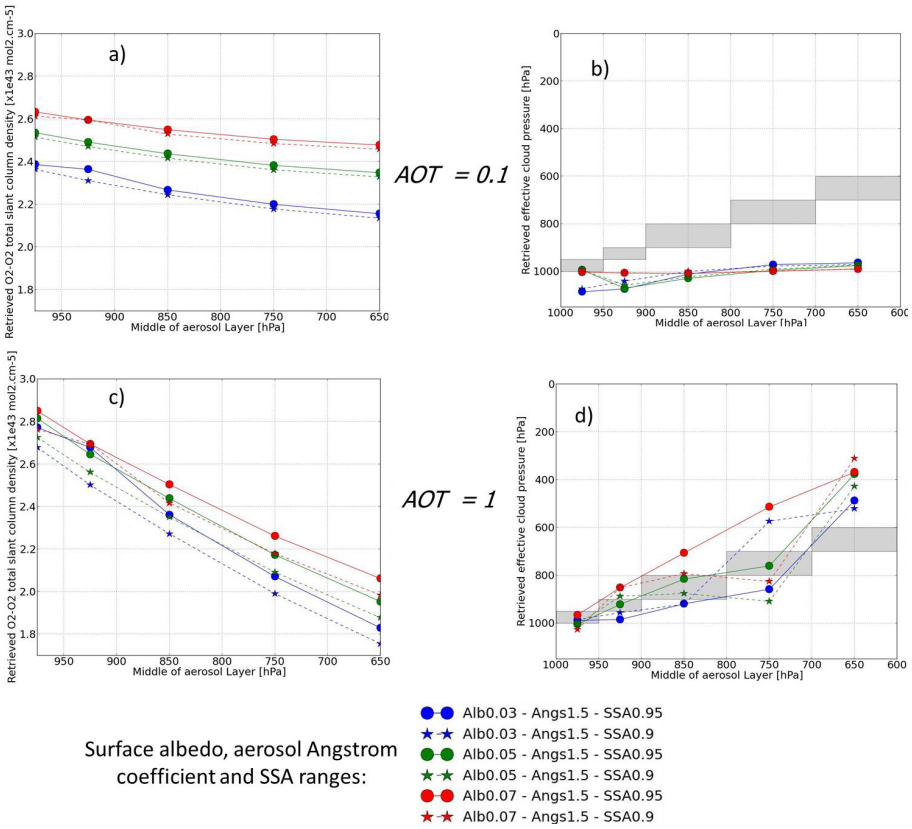

Figure 11. Impact of the location of atmospheric aerosols layers on the simulated DOAS O_2-O_2 cloud retrieval results as a function of AOT and surface albedo. The results are derived from conditions of Fig. 1: **(a)** O_2-O_2 total SCD for AOT = 0.1, **(b)** effective cloud pressure (grey colour depicts the location of the simulated aerosol layers) for AOT = 0.1, **(c)** O_2-O_2 total SCD for AOT = 1, **(d)** effective cloud pressure for AOT = 1.

AMTD
8, 8385–8437, 2015

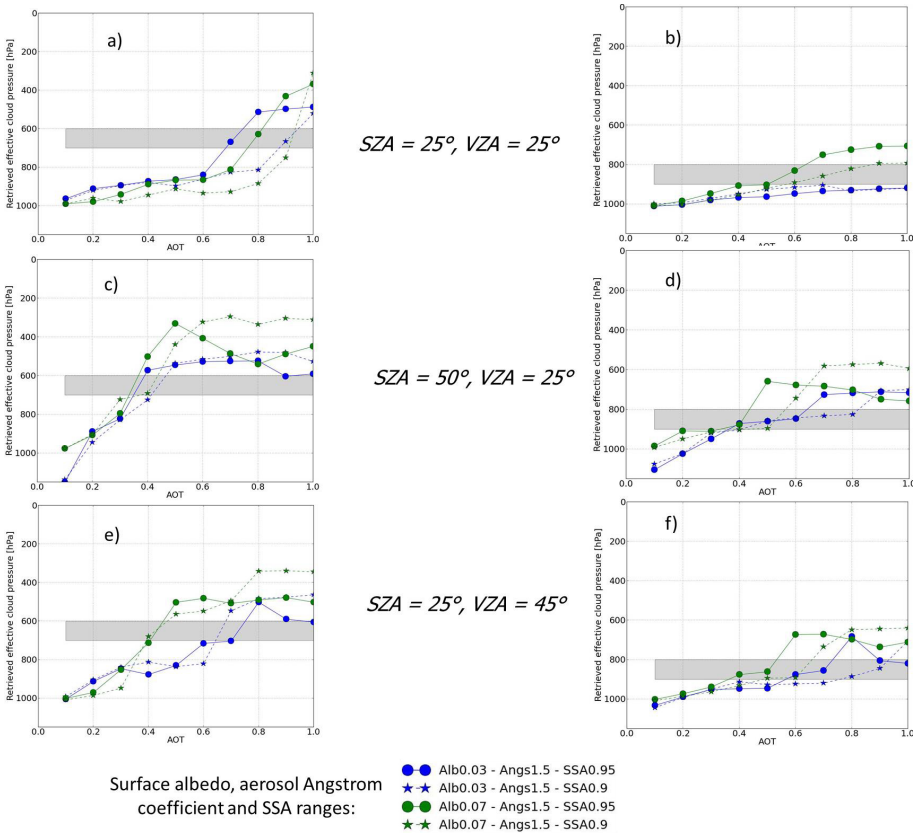

Figure 12. Impact of geometry angles on the effective cloud pressure retrievals as a function of surface albedo, aerosol microproperties, AOT and location of atmospheric aerosol layers (grey colour depicts the location of the simulated aerosol layers). Same conditions than Fig. 1 are assumed: **(a)** and **(b)** SZA = 25° and VZA = 25°, **(c)** and **(d)** SZA = 50°, VZA = 25°, **(e)** and **(f)** SZA = 25°, VZA = 45°.

AMTD
8, 8385–8437, 2015

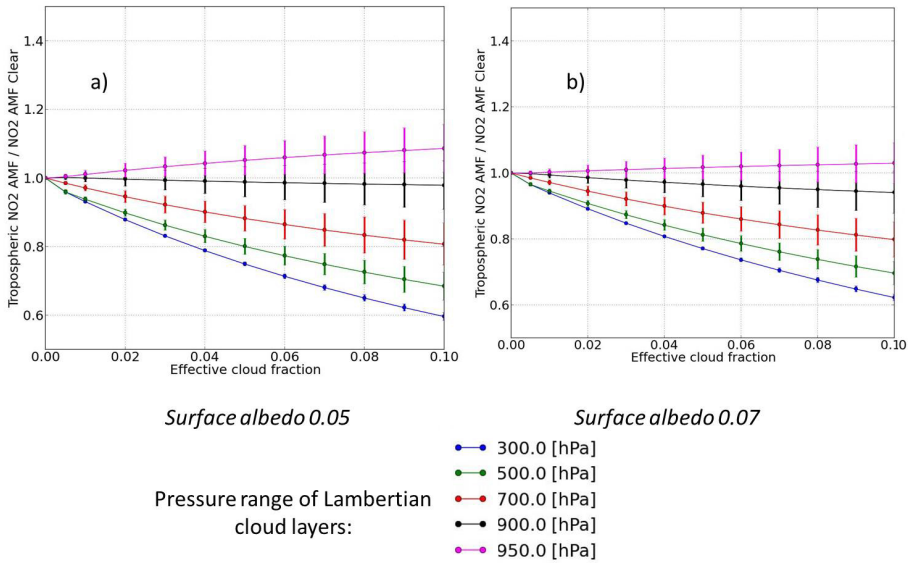

Figure 13. Tropospheric NO_2 AMF factor f at 439 nm (cf. Eq. 5) based on OMI effective cloud parameters (i.e. effective cloud fraction and pressure) and for 2 surface albedos, derived from all the NO_2 vertical profiles from TM5 simulations, 2006, East China, July (cf. Fig. 1). Solid lines are the average, while error bars are the standard deviation, of f computed for all the individual TM5 NO_2 profiles over this period and this region: **(a)** surface albedo 0.05, **(b)** surface albedo 0.07.

AMTD
8, 8385–8437, 2015

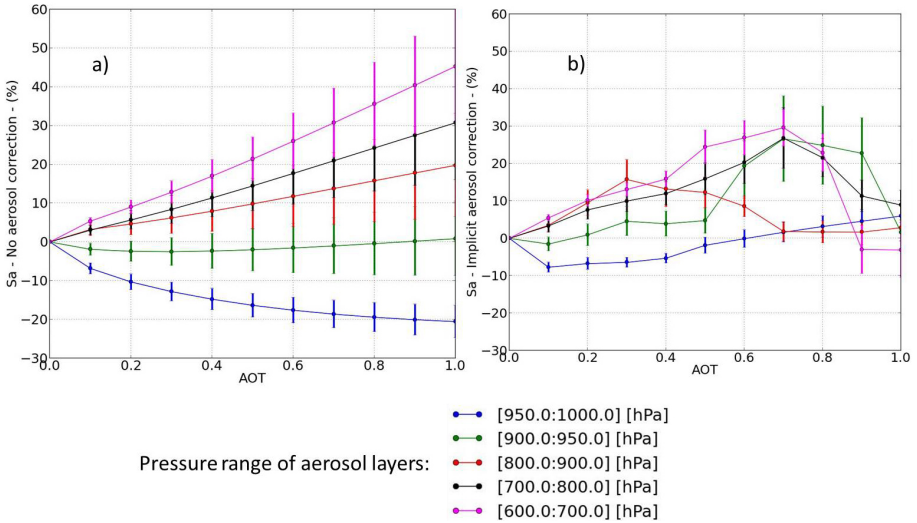

Figure 14. Comparison of relative tropospheric NO_2 AMF biases Sa at 439 nm (cf. Eq. 8) assuming different aerosol atmospheric layers. Aerosol properties are defined by Angstrom coefficient = 1.5, SSA = 0.95, assymetry parameter = 0.7, surface albedo = 0.05, SZA = 25°, VZA = 25°, and TM5 NO_2 vertical profiles for the month of July at 12:00 p.m. over China (see Fig. 1). Solid lines are the average, while error bars are the standard deviation, of Sa computed for all the individual TM5 NO_2 profiles over this period and this region: **(a)** Sa assuming no aerosol correction, **(b)** Sa assuming implicit aerosol correction through the OMI cloud retrieval algorithm.

AMTD
8, 8385–8437, 2015

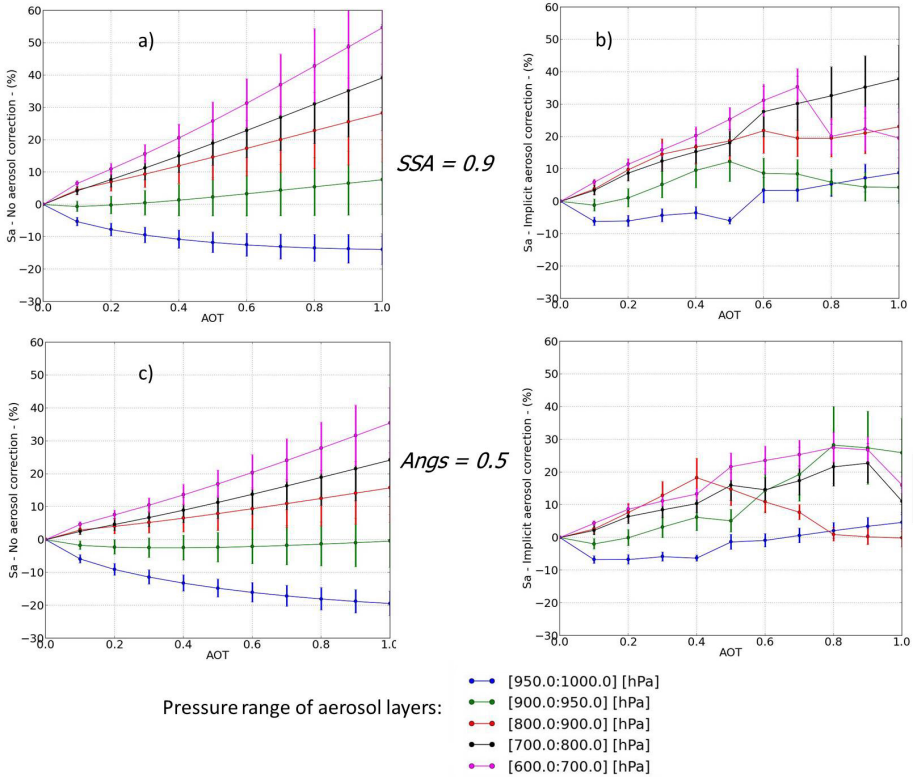

Figure 15. Similar as Fig. 14 but with different aerosols SSA and Angstrom coefficient values: **(a)** Sa assuming no aerosol correction, SSA = 0.9, **(b)** Sa assuming implicit aerosol correction through the OMI cloud retrieval algorithm, SSA = 0.9, **(c)** Sa assuming no aerosol correction is applied, Angstrom coefficient = 0.5, **(d)** Sa assuming implicit aerosol correction through the OMI cloud retrieval algorithm, Angstrom coefficient = 0.5.

AMTD
8, 8385–8437, 2015

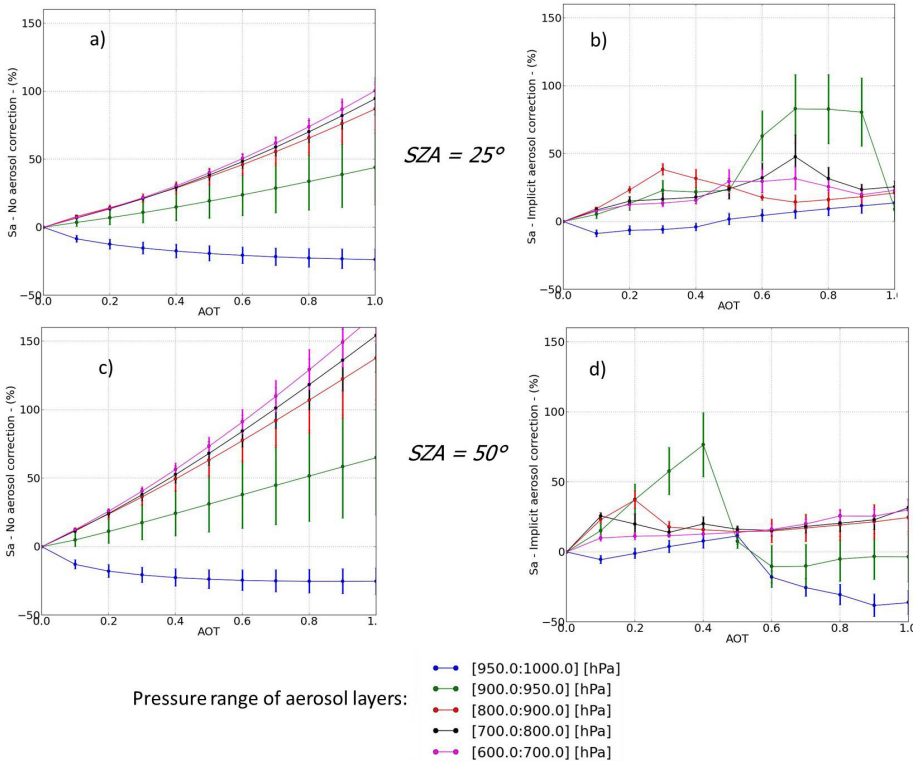

Figure 16. Similar as Fig. 14 but with NO_2 profiles for January and SZA = 50°: **(a)** Sa assuming no aerosol correction is applied, January NO_2 profiles, **(b)** Sa assuming implicit aerosol correction through the OMI cloud retrieval algorithm, January NO_2 profiles, **(c)** Sa assuming no aerosol correction is applied, aerosols, January NO_2 profiles and SZA = 50°, **(d)** Sa assuming implicit aerosol correction through the OMI cloud retrieval algorithm, January NO_2 profiles and SZA = 50°.

AMTD
8, 8385–8437, 2015